

6-13-2014

Cross-Structures and their Role in the Development of the Taiwan Fold-and-Thrust Belt

Ellen A. Lamont

University of Connecticut, ellen.lamont@uconn.edu

Recommended Citation

Lamont, Ellen A., "Cross-Structures and their Role in the Development of the Taiwan Fold-and-Thrust Belt" (2014). *Master's Theses*. 633.
https://opencommons.uconn.edu/gs_theses/633

This work is brought to you for free and open access by the University of Connecticut Graduate School at OpenCommons@UConn. It has been accepted for inclusion in Master's Theses by an authorized administrator of OpenCommons@UConn. For more information, please contact opencommons@uconn.edu.

Cross-Structures and their Role in the Development of the Taiwan Fold-and-Thrust Belt

Ellen Ari Lamont

B.S. Geology, Indiana University of Pennsylvania, 2012
B.A. Geography (GIS), Indiana University of Pennsylvania, 2012

A Thesis

Submitted in Partial Fulfillment of the

Requirements for the Degree of

Master of Science

At the

University of Connecticut

2014

APPROVAL PAGE

Master of Science Thesis

Cross-Structures and their Role in the Development
of the Taiwan Fold-and-Thrust Belt

Presented by

Ellen Ari Lamont, B.S., B.A.

Major Advisor _____
Dr. Timothy Byrne

Associate Advisor _____
Dr. Jean Crespi

Associate Advisor _____
Dr. William Ouimet

University of Connecticut

2014

ACKNOWLEDGEMENTS

It is with great pride that I have finally completed my graduate experience here at the University of Connecticut. But it cannot go unrecognized the great efforts that my friends and colleagues have gone through to get me to this point. Without their encouragement and support, I would not be where I am today. I would first like to thank my advisor, Dr. Timothy Byrne, for his guidance throughout my tenure at UConn. By challenging me to become a better scientist whom always strives for the next opportunity, I have learned how to build a strong network of collaborations and to become involved in the scientific community. I would also like to thank my foreign host and collaborator, Dr. Ruey-Juin Rau, for taking me under wing and providing me with both data and the opportunity to work in his lab in Taiwan. Hosting scholars requires a lot of time and patience, so I deeply appreciate the help I received from you and your students.

To my associate advisors, Dr. Jean Crespi and Dr. William Ouimet, thank you both for aiding me in completing my thesis and for many stimulating, thought-provoking research discussions. Also, thank you Dr. Jonathan Lewis and Dr. Jian-Cheng Lee for your continued correspondence and research discussions which have been insightful and invaluable. To Chung Huang for assistance with GIS problems and shapefiles. To Dr. Kristen Myshrall for editing and reviewing my grant proposals. To Daniel O'Hara for the countless number of brainstorming sessions and thesis drafts he edited. And to the entire UConn geoscience graduate group and our friends in geography for helping keep me on track throughout the entire research/thesis process.

Most importantly, I want to thank the National Science Foundation (Grant 1308896), the Taiwan National Science Counsel, the Geological Society of America and the Center for Integrative Geosciences at UConn for your financial support, as well as, National Cheng-Kung University, National Tsing-Hua University and Academia Sinica for the use of your facilities during my stay in Taiwan. Without your assistance, none of this would have been possible!

TABLE OF CONTENTS

Acknowledgments.....	iii
List of Tables.....	v
List of Figures.....	vi
Abstract	vii
 <u>Cross-structures and their role in the development of the Taiwan fold-and-thrust belt</u>	
Introduction	1
Tectonic Setting	3
Continental Margin of South China	4
Structure of the Taiwan Orogenic Wedge	7
Cross-Structures within the Fold-and-Thrust Belt	9
Sanyi Cross-Structure	10
Pakua Cross-Structure	11
Chiayi Cross-Structure	12
Chishan Cross-Structure	12
Fengshan Cross-Structure	13
Kaohsiung Cross-Structure	13
Methods: Structural Analysis Using Seismicity and Focal Mechanisms	14
Earthquake Seismicity	14
Earthquake Focal Mechanisms	17
Results and Interpretations	22
Seismicity Depth Distribution	22
Focal Mechanism Deformation Styles	22
Stress Inversion and Spatial Analysis Results	23
Margin Control on the Development of the Fold-and-Thrust Belt	29
Conclusion	35
Appendix	36
References	38

LIST OF TABLES

Table 1.	Summary of previous cross-structure investigations by zone	10
Table 2.	Study area box parameters and data	16
Table 3.	Inversion output statistics and parameters	23

LIST OF FIGURES

Figure 1.	Simplified arc-continent collision deformation models (a) Model for hangingwall deformation around a footwall promontory (b) Generalized collision characteristics for the Taiwan collision	2
Figure 2.	Aerial magnetic anomaly map across Taiwan	4
Figure 3.	Isopach maps of the Chinese continental margin	6
Figure 4.	Tectonic setting of Taiwan (a) Morphotectonic setting map (b) Topographic map of the Taiwan orogen	8
Figure 5.	Map of earthquake seismicity and depth distribution plots	15
Figure 6.	Map of focal mechanisms and ternary diagrams of earthquake kinematics	18
Figure 7.	Sanyi study area stress inversion results	24
Figure 8.	Pakua study area stress inversion results	25
Figure 9.	Chiayi study area stress inversion results	27
Figure 10.	Chishan study area stress inversion results	28
Figure 11.	Drainage anomaly map of conjugate faults	31
Figure 12.	Geologic map of Taiwan with suggested tear faults	33
Figure 13.	Oblique arc-continent collision model for fold-and-thrust belt deformation around a crustal promontory in Taiwan	34

ABSTRACT

Traditional models of orogenic growth over-simplify the processes involved in the development of fold-and-thrust belts by failing to take into consideration along-strike irregularities of the collisional footwall. Inherited footwall geometries are fairly common and can drastically alter the shape of an advancing orogen during collision. In Taiwan, the geometry of the Chinese continental margin has been suggested to facilitate the development of several cross-structures, transverse structures that trend oblique to the structural grain of the orogen, within the fold-and-thrust belt. These cross-structures are believed to accommodate deformation around a regional footwall promontory, the Peikang High. In total, six major tear fault zones have been identified in previous studies, though their interpretations are almost exclusively derived from surface deformation studies. For this study, a catalog of earthquake seismicity and earthquake focal mechanisms were used to evaluate and characterize the cross-structures at depth. Using the Gauss inversion method, best-fit stress tensors were derived for each study area and the associated preferred nodal planes of failure were extracted for spatial analyses. Results suggest that deformation patterns north and south of the crustal promontory are characterized by systems of conjugate faulting that facilitate brittle extrusion of foreland material as the orogen becomes caught up in collision with the irregular margin. The region around the promontory represents a narrow zone of southward propagating, en echelon tear faults that accommodate differential displacement of the advancing thrust sheets through time. Tear faulting is limited to the upper crustal layers and are necessary for the orogen to advance over the promontory.

Cross-structures and their role in the development of the Taiwan fold-and-thrust belt

I. Introduction

Arc-continent collisions are fundamental tectonic processes that are partially responsible for the accretion of continental material and orogenic growth. Prevalent around the world, arc-continent collisions have been the focus of numerous investigations (i.e. [Brown *et al.*, 2011; Clift *et al.*, 2003]) that often take a 2-dimensional approach to describing orogen development. This approach utilizes orogen normal profiles containing the interpreted geometry of imbricated thrust sheets, fault-bend folds, and a basal detachment over which the orogen deforms. Such an approach is necessary for understanding orogen development, however, it fails to acknowledge the along-strike deformation presented in a 3-dimensional setting.

Global observations of fold-and-thrust belts indicate that many orogens display a non-linear structural grain [Macedo and Marshak, 1999; Marshak, 2004], highlighting the importance of along-strike variations in orogen development. Orogenic models suggest that these variations can be created by irregularly shaped upper or lower plates. Variations in plate geometries can result in a curvilinear fold-and-thrust belt pattern containing salients and recesses connected by cross-structures (Figure 1a). Cross-structures are structural features trending oblique to the structural grain of the orogen that accommodate differential displacement of the thrust sheets. In this relatively simplified model, these cross-structures trend sub-parallel to the flanks of the promontory and record opposite senses of slip [Marshak, 2004].

Irregularities observed in the footwall of the Taiwan accretionary wedge also appear to strongly influence deformation within the upper plate. The Taiwan orogen is characterized by a well-developed fold-and-thrust belt displaying both salients and recesses (Figure 1b).

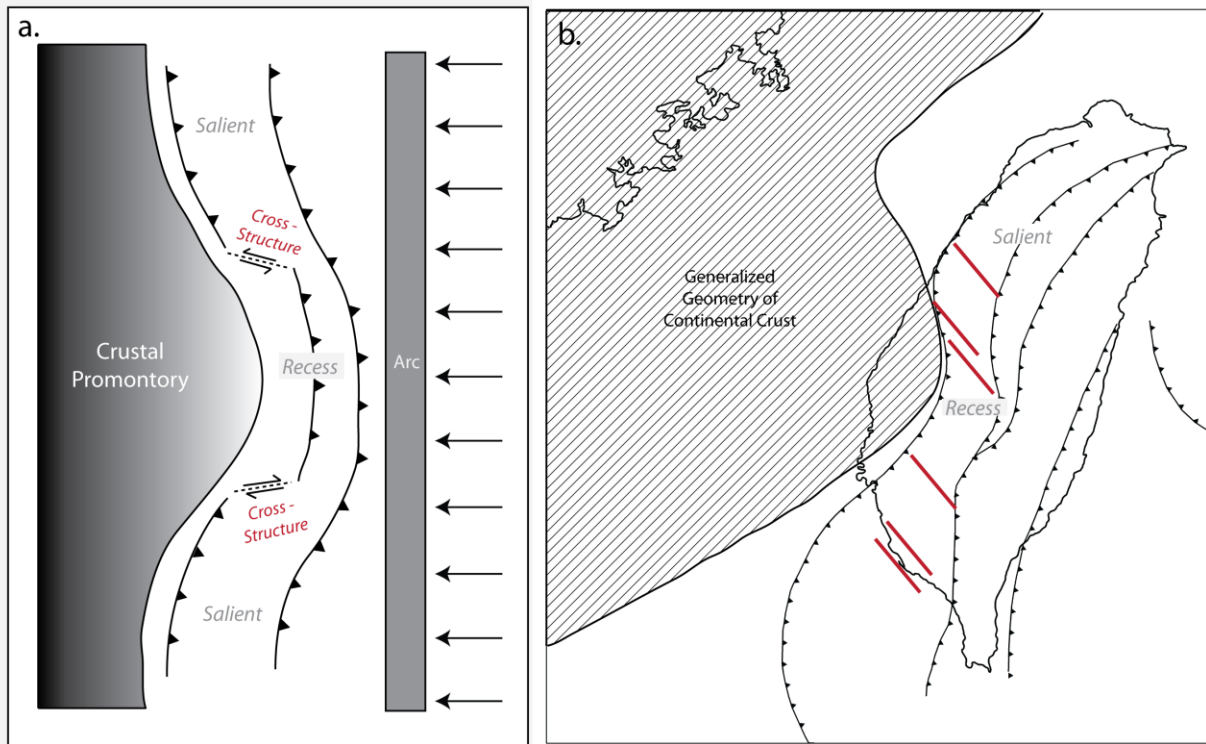


Figure 1. Simplified arc-continent collision deformation models. (a) Model for hangingwall deformation around a footwall promontory (modeled after Marshak, 2004). Black barbed lines - thrust sheet traces with barbs on the hangingwall. Full arrows - convergence direction. Half arrows - fault slip sense. (b) Generalized collision characteristics for the Taiwan arc-continent collision. Black barbed lines - thrust sheet surface traces for major tectonic units with barbs on the hangingwall. Gray filled polygon - approximated geometry of the full-thickness continental crust. Red lines - cross-structures identified by Deffontaines et al., 1997.

The curvilinear nature of the fold-and-thrust belt has been interpreted to result from deformation around a footwall promontory known as the Peikang High. Similar to the simplified model, at least six map-scale cross-structures have been proposed based on geodetic, geomorphic, and geologic field investigations across the fold-and-thrust belt [Deffontaines et al., 1997; Lacombe et al., 1999; Mouthereau et al., 1999]. However, these cross-structures do not parallel the flanks of the crustal promontory and have all been interpreted as having the same (sinistral) sense of slip, contrary to the opposite slip senses expected within the model. The inconsistencies between the cross-structures of the simplified model and the observed cross-structures in the Taiwan orogen raise fundamental questions about orogenic development in relation to the irregular footwall: (1) What is the detailed structure of the crustal promontory; (2) What are these

previously recognized cross-structures in the hangingwall; and (3) How are the cross-structures related to the promontory?

The purpose of this paper is to characterize the nature and geometry of four of the more prominent, previously recognized cross-structures in the Taiwan fold-and-thrust belt, focusing on the distribution of seismicity and kinematics for each zone. The results are more consistent with the general pattern of the simplified model [Marshak, 2004] than previous studies; however, the cross-structures vary significantly along strike. Analyses indicate that only one of the four cross-structures in the Taiwan fold-and-thrust belt behaves as a through-going tear fault, consistent with the simple model. This structure, the Chiayi cross-structures or Luliao, appears to have developed as part of a limited, southward propagating accommodation system that enabled differential emplacement of the fold-and-thrust belt over the thick, crustal promontory. North and south of the promontory, cross-structures form conjugate sets that facilitate along-strike flow around the promontory.

II. Tectonic Setting

The Taiwan orogen is the product of the oblique collision between the north-trending Luzon Arc belonging to the Philippine Sea Plate and the northeast-trending Chinese passive continental margin of the Eurasian Plate [Suppe, 1981]. The contemporary convergence rate for the Philippine Sea Plate with respect to the Eurasian Plate is approximated as 82mm/yr toward 309° [Lee and Chan, 2007; Yu *et al.*, 1997]. The orogen is described as the classic type-model for compressional wedge development [Davis *et al.*, 1983] and is commonly interpreted as Miocene in age (~6Ma) [Taylor and Hayes, 1983]. However, debate over the actual age of collision has arisen in light of several stratigraphic, paleomagnetic, and fission track dating studies that suggest initial collision ages ranging anywhere from 2-6 Ma [Byrne *et al.*, 2011].

Continental Margin of South China

The Chinese continental margin preserves a complicated history of stretching and rifting. Two stages of rifting, an initial phase of southeastward extension (32-30 Ma) and a middle phase of southward extension (30-24 Ma) [Lin *et al.*, 2003], resulted in a complex pattern of thinned rift basins and thick crustal highs along the margin. The effect of rifting is complex and

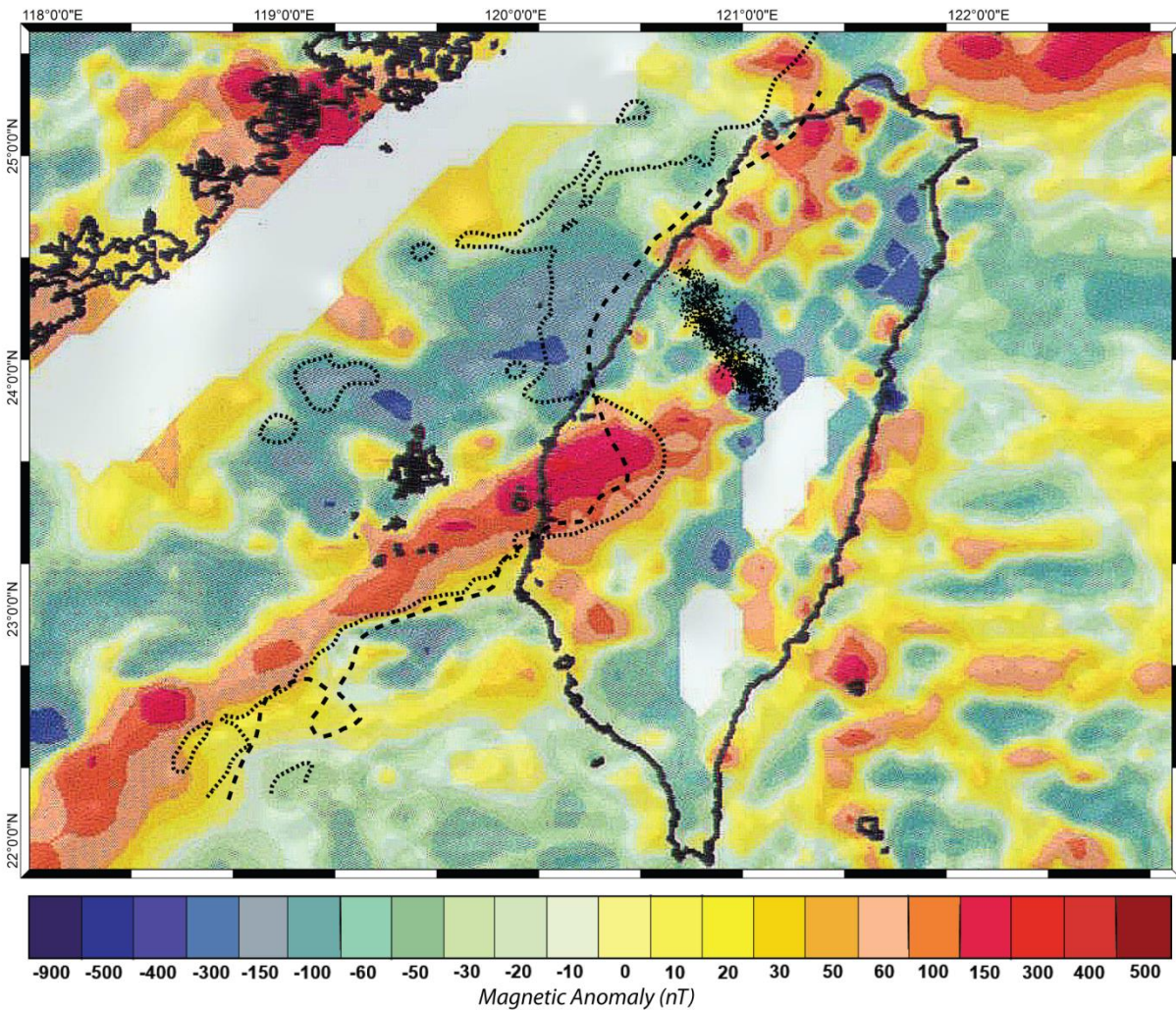


Figure 2. Aerial magnetic anomaly map from across Taiwan (from Wang *et al.*, 2002). Red magnetic high band - interpreted strip of gabbroic rocks defining the edge of the full-thickness continental crust (Cheng, 2004, Hsu *et al.*, 1998, Wang *et al.*, 2002). Black dots - earthquake epicenters within the Sanyi-Puli Seismic Zone from 1991 - 1999. The seismic zone parallels an interpreted footwall fracture zone (Byrne *et al.*, 2011). Black dotted line - 4 km depth contour to the top of the Mesozoic basement (taken from Figure 3a). Black dashed line - 2 km depth contour to the base of the foreland sedimentary sequence (taken from Figure 3b).

observable throughout the crust. Within the lower crust, an anomalous, northeast trending magnetic high belt was discovered through the joint analysis of gravity and seismic velocity data. This magnetic anomaly follows along the northern edge of the Tainan Basin, before truncating beneath central Taiwan (Figure 2), and has been interpreted as the mafic, underplated edge of full-thickness continental crust (~30km) [Cheng, 2004; Hsu *et al.*, 1998; Wang *et al.*, 2002]. Byrne *et al.* [2011] interprets the magnetic high truncation as a continental margin fracture zone that correlates with the Sanyi-Puli Seismic Zone, an anomalously linear, map-view cluster of seismicity.

Within the triangular zone of crust southwest of the fracture zone, seismic reflection and drill core studies yield a detailed isopach map of the Mesozoic Basement, which serves as a proxy for the rifted, shallow continental margin (Figure 3). The isopach map indicates that the Chinese margin is composed of two large basins, the Tashi and Tainan basins, and a bathymetric high composed of full-thickness continental crust, the Peikang High. The Peikang High is a foreland forebulge that separates the en echelon Tashi and Tainan basins and is interpreted to have developed when a sliver of continental crust rotated $\sim 15^\circ$ clockwise away from the margin during the transition from southeast to south directed extension [Lin *et al.*, 2003]. Early rifting in this region is also suggested to be responsible for the establishment of the general northeast trend of the margin [Mouthereau and Lacombe, 2006].

Dissimilar to previous studies that evaluate the magnetic anomaly and the Peikang High as separate structural features, I interpret them as two crustal highs that compose a single, complex marginal promontory. The magnetic anomaly defines a stair-step shaped corner within the lower crust, while the Peikang High represents a broad protrusion at shallow crustal levels. Together, these pieces of the complicated promontory belong to the collisional footwall. I further

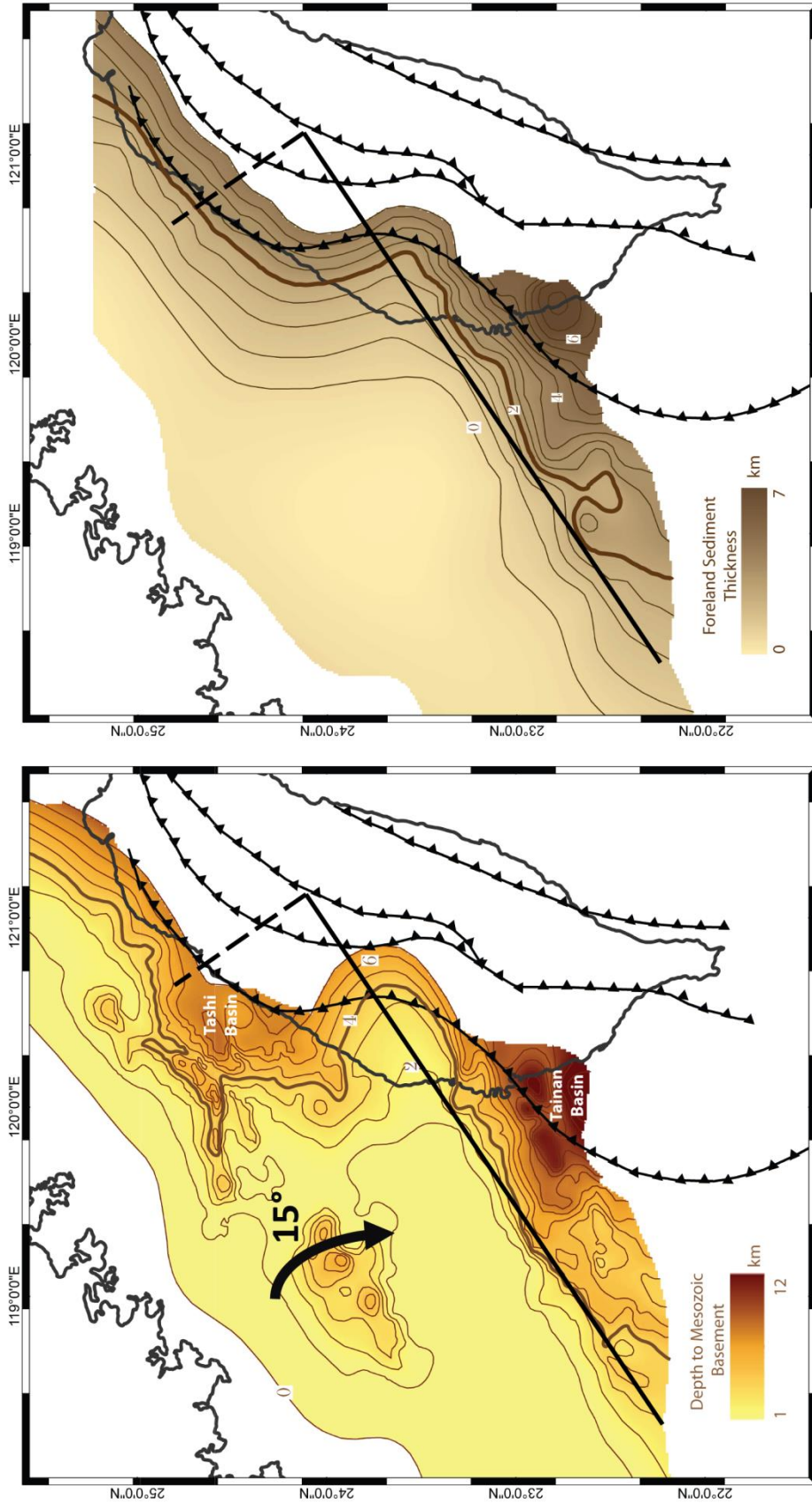


Figure 3. Isopach maps of the Chinese continental margin (adapted from Lin et al., 2003). (Left) Depth to the Mesozoic basement. Contour interval = 1 km. (Right) Depth to the base of the foreland sedimentary sequence. Contour interval = 0.5 km. Bold contours - contour following change in gradient from gentle to steep slope along the unit. Black line - trend of magnetic high from Figure 2. Black dashed line - inferred footwall fracture zone. Black curved arrow - rotation of the Peikang High sliver away from the continent during the change in rift direction from southeast to south.

suggest that the geometry of the Peikang High and the en echelon basins have a direct control on the deposition characteristics of the foreland sediment into which the Taiwan orogen propagates.

Structure of the Taiwan Orogenic Wedge

The Taiwan orogen is composed of five distinct morphotectonic regions from east to west: the Coastal Range, Central Range, Hsüehshan Range, Western Foothills and Coastal Plain, respectively (Figure 4a). Belonging to the Philippine Sea Plate, the Coastal Range is located on the eastern side of the island and represents the collided Luzon Arc and forearc. The remaining four regions belong to the Eurasian Plate and make up the accretionary wedge. These units increase in metamorphic grade from west to east, ranging from loose, undeformed sediments in the Coastal Plain to medium-high grade metamorphic rocks of the eastern Central Range [Ho, 1986]. The focus of this study will be within the Western Foothills where the fold-and-thrust belt is growing across the foreland.

The fold-and-thrust belt contains a series of vertically fanning, west-vergent thrust faults with oblique top-to-the-west motion that progressively deform the foreland sediments over an ~5-10 km basal detachment [Brown *et al.*, 2012; Ho, 1976; Lee *et al.*, 1996]. Along strike, the fold-and-thrust belt is characterized by a curvilinear geometry. In the Tashi Basin, a major salient is evident in the arcuate traces of the thrust sheets and in the curvature of regional folds (Figure 4a). At the northern end of the salient, the structural trend of the fold-and-thrust belt rotates clockwise from a north-northeast trend to a northeast trend [Teng, 1996], nearly parallel with the trend of the northern margin. Approaching the southern end of the salient near the Peikang High, the trend of the frontal Tatushan and Pakuashan anticlines rotates counter-clockwise in a sigmoidal pattern before returning to a northeast trend south of the Peikang High, again parallel to the margin [Deffontaines *et al.*, 1997; Lee *et al.*, 1996; Mouthereau *et al.*, 2001; Mouthereau

et al., 1999]. The deviation in the trend of the frontal anticlines serves to link the northern fold-and-thrust belt to the southern extension which is characterized by dominantly northeast striking folds and faults. Modern states of stress suggest that many of these faults may be reactivated as oblique, right-lateral thrust faults [Lacombe *et al.*, 2001].

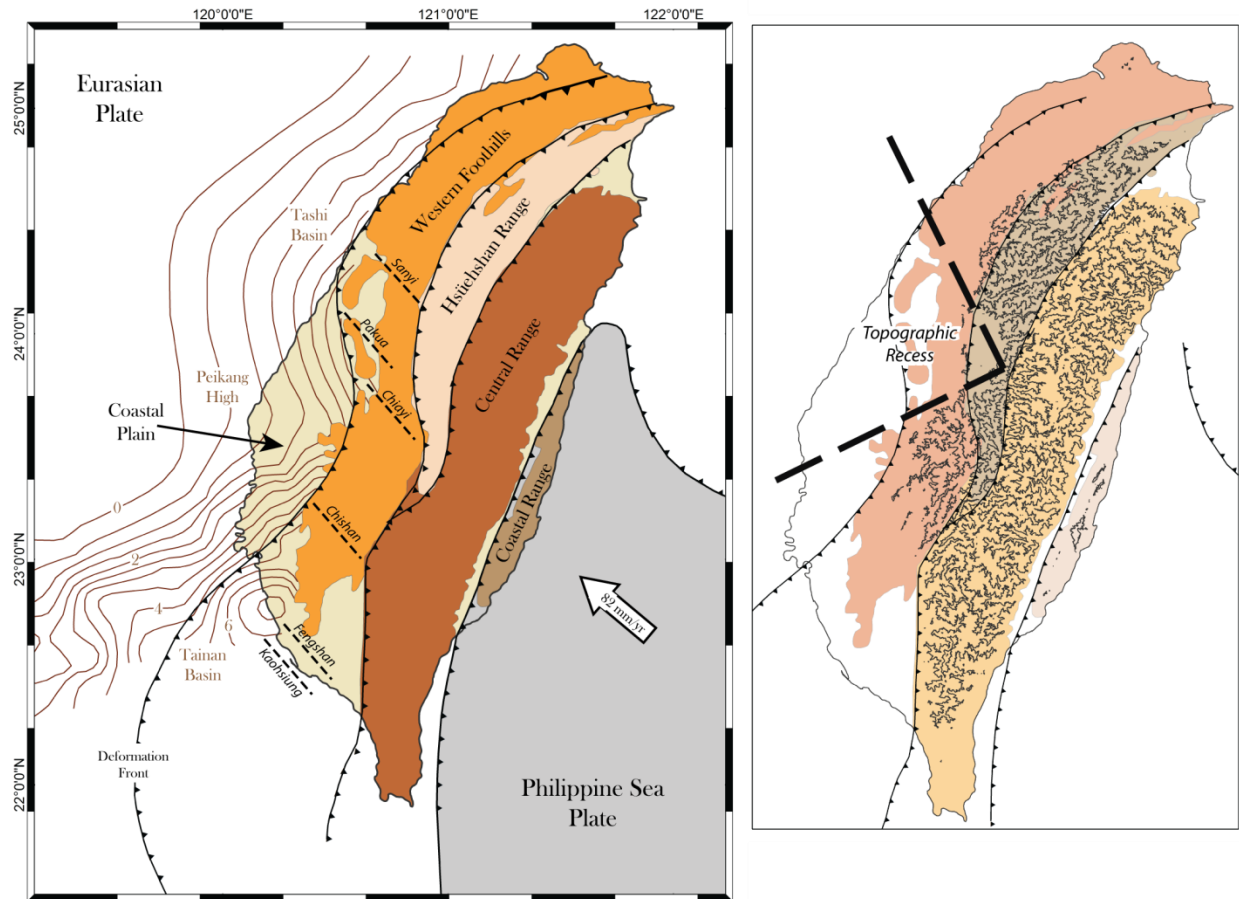


Figure 4. Tectonic setting of Taiwan. (a) Morphotectonic setting map (adapted from Ching *et al.*, 2011). Brown lines - depth to the base of the foreland sequence in kilometers (from Figure 3) (Lin *et al.*, 2003). Black barbed lines - thrust sheet traces with barbs on the hangingwall. Black dashed lines - cross-structures (from Deffontaines *et al.*, 1997). While arrow - Philippine Sea Plate convergence vector toward 309°. (b) Topographic map of the Taiwan orogen. Contours derived from the Taiwan 40 m DEM. Contour interval = 1000 m. Black dashed lines - inferred lower-crustal promontory from Figure 2.

Also of note is the topographic pattern across the western Hsüehshan Range and central fold-and-thrust belt. An S-shaped topographic map pattern is observed in the vicinity of the magnetic anomaly/fracture zone (Figure 4b) and is emphasized by an abrupt muting of the topography along the Sanyi-Puli seismic zone. One of the most obvious features of this

topographic anomaly is the a large, low relief basin nestled within the mountains of the Hsüehshan Range, the Puli Basin, which is situated at the apex of two sides of the s-shape [Mirakian *et al.*, 2012]. Beyond this topographic recess, the fold-and-thrust belt has continued to propagate westward. Taking both the major salient and the topographic recess into consideration, I suggest that the geometry of the complex promontory has considerable control over the development of the orogen. The effect of the promontories on the orogen can be directly observed as the fold-and-thrust belt deforms to partially contour to the shape of the promontory at both crustal levels, creating salient and recess configurations similar to that proposed by the simple model.

III. Cross-Structures within the Fold-and-Thrust Belt

Several studies were conducted to identify and investigate cross-structures within the Taiwan fold-and-thrust belt. These structures have been described as transfer faults, lateral ramps and tear faults in the literature. However, these accommodation structures will simply be referred to as cross-structures herein. In all, six northwest trending, sinistral cross-structures have been inferred. Cross-structures in Taiwan were first recognized by Deffontaines *et al.* [1997] using digital elevation models, in conjunction with slope and hillshade maps, to highlight anomalous topographic and drainage lineaments across the Western Foothills. Anomalies were extracted and analyzed for relevant structural patterns, accounting for known topographic features such as major faults and fold axes. From these, several anomalies were identified trending oblique to the structural grain of the fold-and-thrust belt. These cross-structures have been proposed as a series of N140E striking features corresponding approximately to the regional convergence direction [Deffontaines *et al.*, 1997; Lacombe *et al.*, 1999; Mouthereau *et al.*, 1999]. From north to south, these cross-structures are: Sanyi, Pakua, Chiayi (or Luliao), Chishan, Fengshan, and Kaohsiung

cross-structures (Figure 4a). The following sections summarize the subsequent cross-structure investigations conducted in Taiwan (Table 1). A wide range of geomorphic, geologic, and geodynamic techniques were utilized in the identification of these features, each employing methods that focus exclusively on deformation observed at or near the surface as a means of inferring information about the zones at depth.

Table 1. Summary of cross-structure evidences from previous studies. Information is from Ching et al., 1997; 2011; Deffontaines et al., 1994; 1997; Lacombe et al., 1999; Mirakian et al., 2012; Mouthereau et al., 1999.

	STFZ	PTFZ	CTFZ	ChiTFZ	FTFZ	KTFZ
Size	100 km Long	--	--	20 km Long	~40 km Long	--
Fault Zone Trend	N140E	N140E	N110E	N140-160E or N130E	N140E	N140E
Sense-of-Slip	Left Lateral	Left Lateral	Left Lateral	Left Lateral	Left Lateral	Left Lateral
Identified by Geomorphology	Drainage Anomalies	Drainage Anomalies	Drainage Anomalies	Drainage Anomalies	Drainage Anomalies	X
Identified by Field Data	N140E/N80E trending joints	N140E/N80E trending joints	Offset Deformation front conglomerates	Sinistrally sheared clays & shear cleavage	N140E/N80E trending joints	N140E/N80E trending joints
Structural Evidence	Southern Termination of CPC Tiehchanshan Oil/Gas Field	Anticline Axis Virgation between Tatu & Pakua Anticlines	--	Sigmoidal Thrusts & Fold Axes, Offset Deformation Front, + Flower Structure	Sigmoidal Thrusts, Fold Axes and Reef Systems	Rectilinear Shoreline
Identified by Seismicity	Seismic Density Boundary	--	Linear cluster of events following Chi-Chi Earthquake	Seismic Density Boundary	--	--
Identified by GPS	--	--	Differential Displacement	Differential Displacement	Differential Displacement	--
GPS Displacement	--	--	NE Block: 33mm/yr SW Block: 26mm/yr	NE Block: 18.5 mm/yr SW Block: 7.5 mm/yr	NE Block: 13 mm/yr SW Block: 7.5 mm/yr	--
Other Displacement	--	--	--	6 km of slip: 12 +/- 4mm/yr	~5.5 mm/yr or 6 +/- 1 mm/yr	--
Mechanism	Pure Strike-Slip Faulting	Transtensive: Normal (south) Reverse (north)	Transpressive Reverse	Transpressive Reverse	Transtensive Normal	--
Cause	Northern Boundary of Peikang High	Peikang High & Thrusting over Oblique Lateral Ramp	Peikang High Buttress & Thin Sediments	Lateral Ramp & Change in Sedimentary Thickness	Peikang High & Change in Sedimentary Thickness	--

Sanyi Cross-Structure

Studies conducted in the area rely heavily on earthquake and structural investigations to delineate the Sanyi cross-structure. The Sanyi zone is easily defined as a seismic boundary between a highly seismic region to the northeast and a nearly aseismic region to the southwest

[Deffontaines *et al.*, 1997]. This zone became illuminated as a well-defined, linear seismic cluster of low magnitude earthquakes during the eight years of seismic monitoring in Taiwan preceding the 1999 Chi-Chi Earthquake, a devastating M_L 7.6 event that struck central Taiwan [Kao and Chen, 2000]. This band of seismicity parallels the Chinese margin fracture zone interpreted by Byrne *et al.* [2011], from the aerial magnetic data of Wang *et al.* [2002], suggesting that the fracture zone may have been reactivated at depth along the Sanyi zone. This is further supported by the identification of two clusters of seismicity at depth; a shallow, upper crustal cluster at 5-15 km (spanning the décollement level) and a second deeper cluster at 20-35 km (consistent with the depth of the fracture zone) [Byrne *et al.*, 2011]. Kinematic analyses of focal mechanisms from within the Sanyi zone suggest that it is a N140E trending, left-lateral fault zone. The existence of this zone has been further suggested by structural investigations, citing the curvilinear nature of fold axes and thrust sheet traces near the fault zone in addition to the mismatching of structures on either side of the cross-structure. For example, the Chinese Petroleum Company Tiehchanshan anticline oil and gas field terminates at its southern end due to apparent truncation by the Sanyi cross-structure [Deffontaines *et al.*, 1997].

Pakua Cross-Structure

Using the same drainage anomaly analysis of Deffontaines *et al.* [1997], a series of NW-SE trending lineaments were detected across the Pakuashan anticline [Lee *et al.*, 1996]. These anomalous drainages trend oblique to the trend of the dip slope and are guided by a series of N140E structural joints in the anticline. Progressive curvature of the Tatushan and Pakuashan anticlines from N10E to N20W southward [Mouthereau *et al.*, 1999] has been argued to be facilitated by field-measured N140-150E left-lateral and N80-90E right-lateral conjugate faults that act as a wrench zone [Deffontaines *et al.*, 1997]. Lee *et al.* [1996] proposed that these

conjugate faults were part of a major left-lateral shear/fault system positioned through the northern segment of the Pakuashan anticline, causing plan-view asymmetry of the fold.

Chiayi (Luliao) Cross-Structure

The Chiayi cross-structure has been recognized in a variety of geomorphic, geodetic, and seismologic investigations, though it remains elusive in most field and surficial studies. This zone has been recognized in drainage anomalies as well as in Side-Looking Airborne Radar imagery where it is interpreted to laterally offset the conglomerates along the deformation front [Deffontaines *et al.*, 1994; Deffontaines *et al.*, 1997]. GPS velocities derived from Taiwan's dense station array yields displacement values of 33mm/yr toward the west, northeast of the zone and 26mm/yr toward the west, southwest of the zone, indicative of differential, left-lateral displacement across the structure. It has also been suggested that the Chiayi cross-structure is responsible for the offset of fold axes and curvature of the Chukou Thrust Fault [Deffontaines *et al.*, 1997]. Seismically, the Chiayi zone became intensely illuminated for a few hours following the 1999 Chi-Chi Earthquake. Closer inspection of these events revealed that the zone created a steeply dipping, planar seismic zone with events that propagated 50 km to the southeast along the zone through time [Rau *et al.*, 2008].

Chishan Cross-Structure

Similar to the Sanyi cross-structure, the Chishan cross-structure is identified as a major seismic boundary between a northeastern seismic and a southwestern aseismic zone [Deffontaines *et al.*, 1997; Lacombe *et al.*, 1999]. The Chishan zone is also well expressed in geodetic and structural data. Structurally, the existence of the Chishan cross-structure as a tear fault zone has been speculated due to the sigmoidal shape of thrust sheet traces and fold axes

across the zone, the mismatching of folds, the measurement of faults indicating both left-lateral, N130E and right-lateral, N50-80E conjugate sets, and the identification of probable positive flower structures associated with strike-slip faulting [Deffontaines *et al.*, 1997; Lacombe *et al.*, 1999]. Evidence at the outcrop scale of black sheared clays within a light gray, N130-140E striking mudstone unit with penetrative shear cleavage further advocates for tear faulting in this region [Lacombe *et al.*, 1999]. Side-Looking Airborne Radar imagery shows left-lateral offset of the deformation front along the NW-SE branch of the Tsengwen River immediately north of the Chishan cross-structure. Furthermore, GPS displacements of 18.5 mm/yr toward the west, northeast of the zone and 7.5 mm/yr toward the west, southwest of the fault zone indicate differential displacement of the thrust sheets across the zone [Deffontaines *et al.*, 1997; Lacombe *et al.*, 2001].

Fengshan Cross-Structure

Deffontaines *et al.* [1997] and Lacombe *et al.* [1999] both propose the existence of the Fengshan cross-structure, though geomorphic evidence is limited. This zone is most prominently realized by the differential displacement observed across the structure. GPS velocities northeast of the structure show westward displacement of 13 mm/yr and only 7.5 mm/yr of westward displacement southwest of the structure. Curvature and mismatch of fold axes and thrust traces in addition to offset of rare Pleistocene reefal complexes ($\sim 6 \pm 1$ mm/yr) support the notion of faulting along the Fengshan cross-structure [Deffontaines *et al.*, 1997].

Kaohsiung Cross-Structure

Evidence pertaining to the existence of the Kaohsiung cross-structure is limited making it difficult to assess the probability of its existence. The Kaohsiung zone is suggested to follow the

rectilinear shoreline off of Taiwan's southwest coast, following mapped N140E fracture sets. The only onshore evidence for across-structure here is the sigmoidal shape of the Shaoshan Hill reefal deposit [*Lacombe et al.*, 1999].

IV. Methods: Structural Analysis using Seismicity and Focal Mechanisms

Characterization of the proposed cross-structures using a collection of earthquake data is necessary to constrain the geometry, spatial distribution and kinematics of each zone at depth. In the following sections, a collection of earthquake data, including earthquake foci and earthquake focal mechanisms, is presented from across Taiwan and inverted for the best-fit stress tensor for each study region. From these inversions, the preferred nodal plane of failure, representing the likely geometry of the earthquake-associated fault, is determined and assessed for spatial relationships.

Earthquake Seismicity

The Central Weather Bureau Seismic Network yields an extensive catalog of earthquake data from around Taiwan. On average, the network records more than 15,000 earthquake events per year, approximately one third of which are located in the Western Foothills [*Mouthereau and Lacombe*, 2006]. The seismicity data represents a collection of earthquake foci, collected from 1991 to 2012, for which only the timing, geographic coordinates, depth, and magnitude are known. These events were precisely relocated using the 3D Velocity Model of Rau and Wu [1995] which has an associated error of +/- 3km horizontally and +/- 5 km vertically.

Definition of the Study Areas

Subsets of seismicity data were extracted spatially using a series of N140E trending boxes (Figure 5) with positions and dimensions defined by both physical and spatial parameters

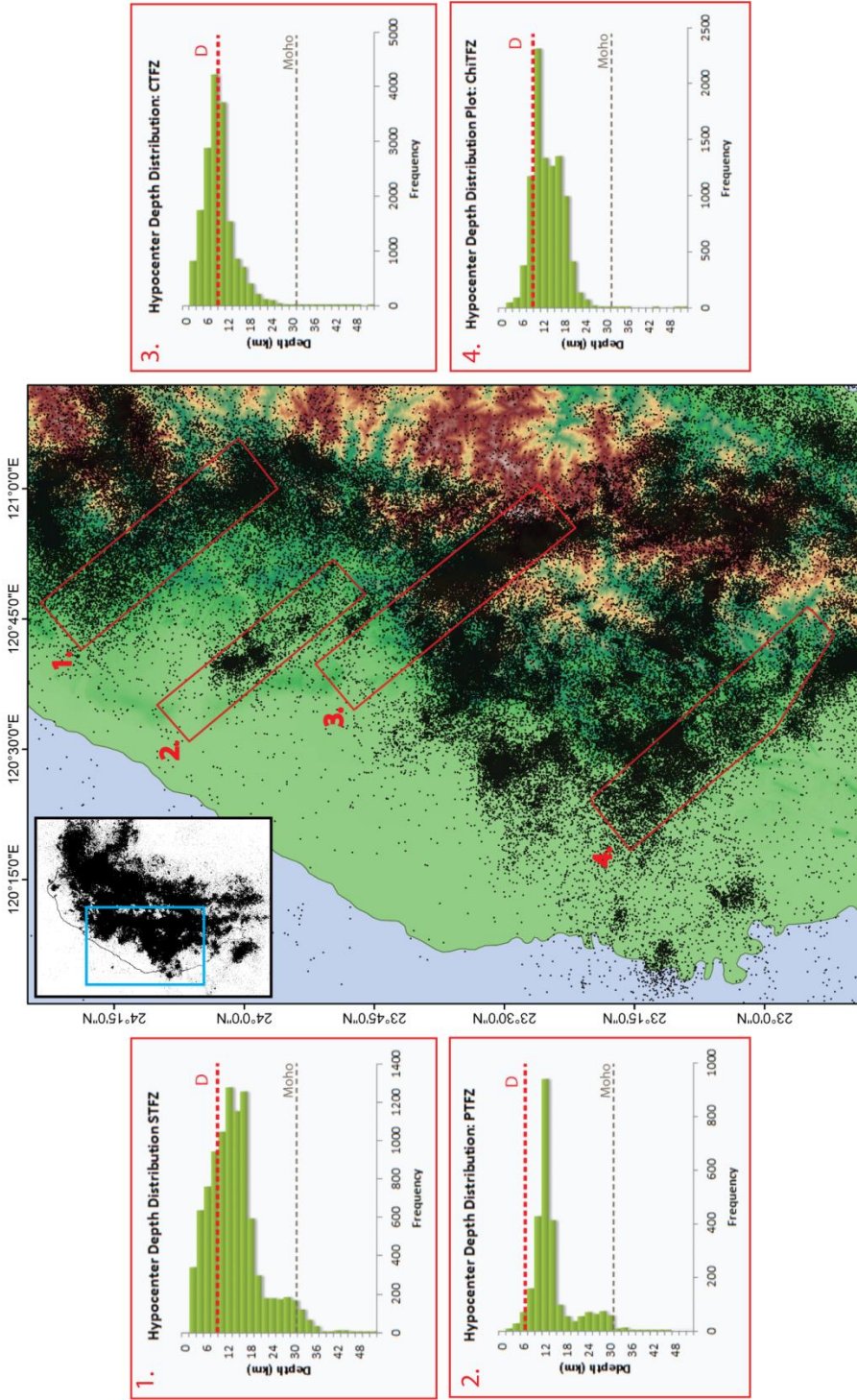


Figure 5. Map of earthquake seismicity and earthquake depth distributions. Data from Taiwan Central Weather Bureau Seismic Network for the period from 1991-2012 and were relocated using the 3D Velocity Model of Rau and Wu, 1995. Map: Black dots - individual earthquake events. Red boxes - Study areas from which data was extracted. Boxes all trend N140E following Deffontaines et al., 1997. Depth Histograms: Frequency of earthquake events plotted by depth (2 km intervals). Gray dashed lines - average depth of the Moho under the fold-and-thrust belt (~30 km). Red dashed line - estimated depth to the fold-and-thrust belt basal detachment taken from Huang et al., 2004.

Table 2. Study area extraction and earthquake data information for each of the cross-structures

Name	Abbreviation	Location	Dimensions from Seismicity	Trend	# of Earthquakes	# of Focal Mechanisms	Seismicity Depth Range	Focal Mechanism Depth Range
Sanyi	STFZ	Between Sanyi - Puli	~ 52.5km L X 12.0km W	N140E	9458	161	0 - 56 km (most = 2 - 17 km)	0 - 43 km (most = 6 - 17 km)
Pakua	PTFZ	Between Dadu - Nantou	~ 25.5km L X 10.0km W	N140E	2576	314	1 - 44 km (most = 8 - 14 km)	3 - 33 km (most = 9 - 13 km)
Chiayi	CTFZ (A.K.A. Luliao)	Between southern end of Pakua Anticline and Alishan Mountain	~ 43.0km L X 10.0km W	N150E	17426	289	0 - 58 km (most = 2 - 12 km)	0 - 27 km (most = 2 - 11 km)
Chishan	ChiTFZ	North of Tainan - Meinong	~ 57.5km L X 12.0km W	N140E	9635	189	0 - 62 km (most = 7 - 19 km)	5 - 25 km (most = 8 - 21 km)
Fengshan	FTFZ	Between Southern Tainan and Nanzhou (Pingdong Plain)	N/A	(N140E)	0	0	N/A	N/A
Kaohsiung	KTFZ	Off-shore Kaohsiung (Follows coastline)	N/A	(N140E)	0	0	N/A	N/A

for each of the four study areas (Table 2). Appropriate boundaries for the Sanyi cross-structure were most evident in spatial-temporal evaluations of the data -- the southern bound was easily defined by a major aseismic zone south of the cross-structure while earthquake events observed from 1991-1999 were used to discern the width of the zone (~12 km), thus establishing the northern bound. Selection of the Pakua and Chiayi study areas was completed by grouping seismic data, with each area's bounding box having a width of ~10 km. The Pakua cross-structure is composed of aligned seismic clusters along the eastern flank of the Pakuashan anticline, and the Chiayi cross-structure is defined by a dense band of seismicity extending eastward from the southern end of the anticline. Similar to the Sanyi cross-structure, the southern bound of the Chishan cross-structure is illuminated by the abrupt boundary created by a major aseismic zone south of the cross-structure, with a slight adjustment made to follow the break in seismicity. Due to the lack of an obvious spatial or temporal boundary to the north, the maximum observed width from the zones (~12 km) was applied to the Chishan cross-structure. None of the zones extend westward beyond the deformation front. The Fengshan and Kaohsiung cross-structures were excluded from analysis as their location in the southern aseismic zone yielded an insufficient amount of data for evaluation.

Vertical Distribution of Earthquake Foci

The distribution of earthquakes is important when determining where in a collisional system active deformation is occurring. In a traditional thin-skinned collision, it is expected that the majority of the deformation, and in turn the seismic activity, occurs above the décollement level. Since Taiwan is often interpreted as a thin-skinned collision [Davis *et al.*, 1983; Ding *et al.*, 2001], cross-structures, such as those in the aforementioned simplified model, should occur at the upper crustal level, above the regional décollement.

Depth histograms were created to assess the vertical distribution of all earthquake events within each study area. Earthquake frequencies were plotted by depth in 2 km bins. Indicator lines were included in the plots, referencing both the depth to the interpreted regional décollement and the depth to the Mohorovičić discontinuity (Moho), which is ~30km beneath western Taiwan [Mouthereau and Lacombe, 2006]. The regional décollement represents the interpreted depth to the base of the orogenic wedge around each study area and was determined from balanced cross-sections created by the Chinese Petroleum Company [S-T Huang *et al.*, 2004].

Earthquake Focal Mechanisms

Earthquake focal mechanisms are useful for constraining kinematics, because they describe the inelastic deformation that occurs during a given seismic event. To evaluate kinematics, a catalog of earthquake focal mechanism solutions was derived from seismicity data from the Taiwan Central Weather Bureau Seismic Network. These events range from 1991-2012, were precisely relocated using the 3D Velocity Model of Rau and Wu [1995] and have an error of +/- 3km horizontally and +/- 5 km vertically. The focal mechanisms were extracted for each study area using the same bounding boxes as described above (Figure 6). In addition to time,

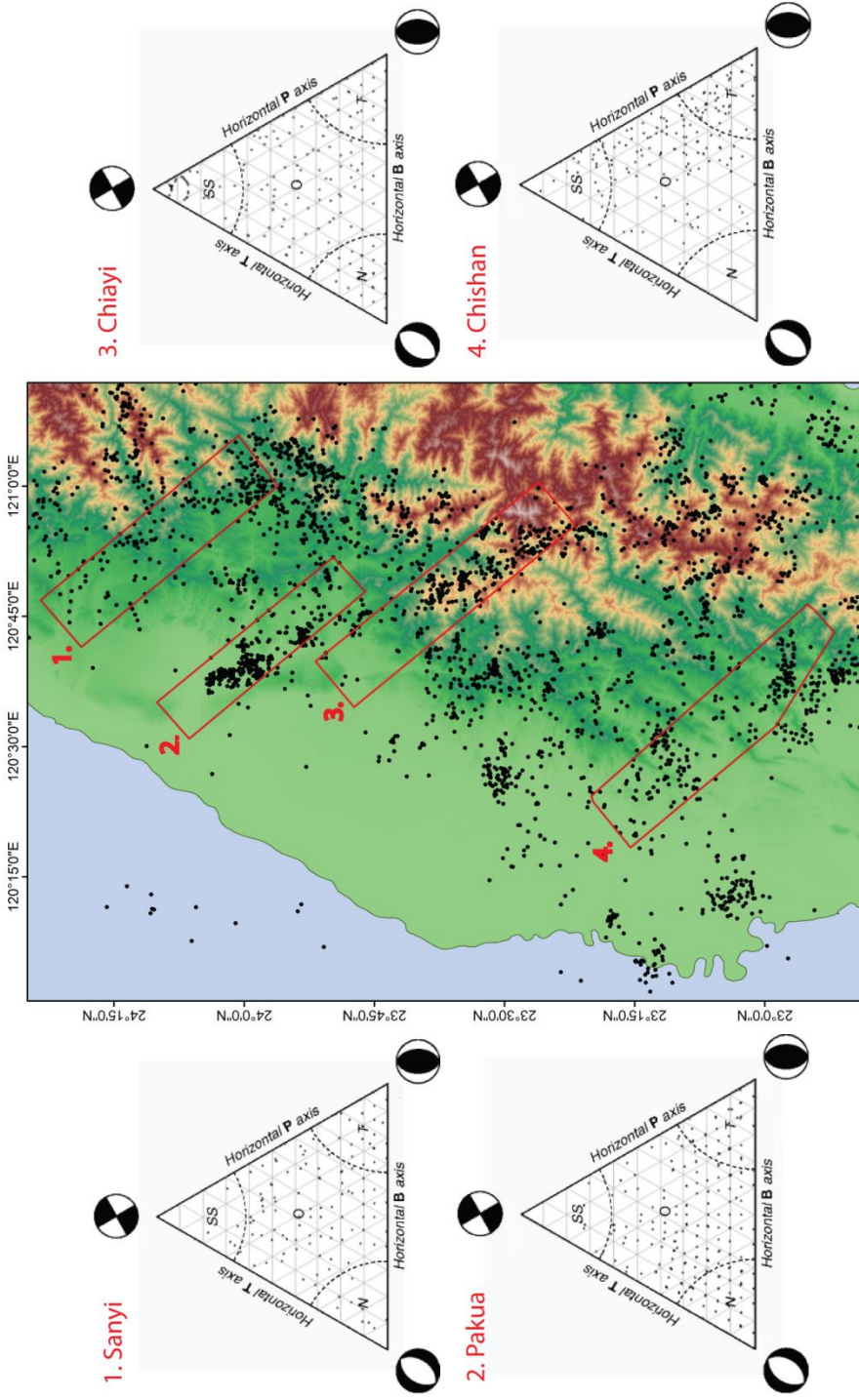


Figure 6. Map of earthquake focal mechanisms and ternary diagrams of focal mechanism kinematics. Data from Taiwan Central Weather Bureau Seismic Network for the period from 1991-2012 and were relocated using the 3D Velocity Model of Rau and Wu, 1995. Map: Black dots - individual earthquake events. Red boxes - Study areas from which data was extracted. Boxes all trend N140E following Deffontaines et al., 1997. Ternary Diagrams: Plots of the plunge angle of earthquake focal mechanism P, T, and B strain axes. N - Normal Fault. T - Thrust Fault. SS - Strike-Slip Fault. O - Oblique Fault. Curved dashed lines - outlet limit of each fault type (Normal and strike-slip limit is 60° and the thrust limit is 50°).

geographic location, depth and magnitude, each earthquake focal mechanism also contains: strike, dip, and rake of both nodal planes and the trend and plunge of the compressional (P), extensional (T), and neutral (B) axes.

Focal Mechanism Ternary Plots

Ternary diagrams are created to depict the P, T, and B axes of each earthquake focal mechanism as they relate to a given deformation style. Each event is plotted within a triangular grid based on the values of the associated P, T, and B axes. Each side of the triangle is assigned as a P, T, or B axis with a value of 0°. The apex of the triangle opposite of a given side has a value of 90°. Earthquakes with B or P-axis values within 30° of vertical (60°-90°) indicate strike-slip or normal faulting, respectively, while earthquakes with T-axis values within 40° of vertical (50°-90°) indicate thrust faulting [Frohlich, 1992]. All other values outside of these ranges suggest oblique faulting.

Stress Inversion and the Best-Fitting Nodal Planes

The goal of a stress inversion is to determine a single tensor that can explain the direction of observed slip on a collection of fault planes. The inversion provides an estimation of the three principal stress axes (σ_1 = maximum compression, σ_2 = intermediate compression, and σ_3 = minimum compression) that define a stress ellipsoid. The ellipsoid represents the most likely stress regime that could have caused the suite of faults to develop [Žalohar and Vrabec, 2007]. Several methods for obtaining the best-fit stress tensor have been developed (e.g. [Angelier, 1990; Angelier et al., 1982; Célérier et al., 2012; Gephart and Forsyth, 1984; Q Huang and Angelier, 1989; Michael, 1987; Žalohar and Vrabec, 2007]) and require that the slip direction of the fault plane and the direction of maximum shear stress are parallel. Because of this requirement, the inversion methods determine a common stress tensor for a homogeneous fault

system that satisfies the requirement by minimizing the misfit angle between the fault slip vector and direction of maximum shear stress for a given trial tensor [Gephart, 1985]. However, it is very uncommon to have a completely homogeneous dataset; therefore, special consideration must be given when analyzing the dataset so that appropriate stress tensors can be determined.

The Gauss inversion method addresses the problem of heterogeneous datasets by providing a way to mathematically divide the dataset into homogeneous subsystems [Žalohar and Vrabec, 2007]. This method considers both the angular misfit and the ratio between normal and shear stress on the fault plane as part of a Gaussian function. The function serves as a measure of compatibility for the dataset where the data fall within a Gaussian distribution. The fit of the data into the Gaussian distribution can be controlled by a series of user-defined parameters that include ϕ_1 and ϕ_2 (which control the normal-to-shear stress ratio), the standard deviation of the angular misfit (s), and the threshold value of compatibility (d) (which is equal to the maximum angular misfit). The values of s and d , when manipulated, control the size and shape of the Gaussian curve; consequently, largely heterogeneous datasets require higher values of s and d to produce meaningful subsets. For each fault tested, if the misfit value is less than the maximum angular misfit defined by the Gaussian function, then the fault is considered compatible. Faults that fall outside of the prescribed range are thus incompatible and tested again with a different stress tensor. This process of testing faults with a trial tensor is repeated until the number of compatible faults is maximized and the angular misfit is minimized.

While the Gaussian inversion method is described for use with fault plane slickenside data, it has direct application to earthquake focal mechanisms and, as a byproduct, is able to select a preferred nodal plane of failure using the best-fit stress tensor. Focal mechanisms are more difficult to invert because of the inherent ambiguity of the nodal planes [Gephart, 1985].

Each focal mechanism is represented by two nodal planes whose significance is equal and interchangeable. During the inversion process, each nodal plane is tested against the trial tensor individually and the nodal plane yielding the lowest misfit value is taken to be the fault plane [C  lerier *et al.*, 2012;   alohar and Vrabec, 2007]. Once a best-fit stress tensor is determined using the previously described process, the preferred nodal planes are selected for the modeled stress tensor and represent the plane from each focal mechanism that best minimizes the angular misfit. The misfit criterion has been used in several studies, each using slightly different algorithms, to select the preferred nodal plane of failure and to test for reliability [Carey-Gailhardis and Louis Mercier, 1987; C  lerier *et al.*, 2012; Gephart, 1985; Gephart and Forsyth, 1984; Harmsen and Rogers, 1986; Michael, 1987;   alohar and Vrabec, 2007; Zoback, 1992].

Using the Gauss inversion method, the earthquake focal mechanisms extracted from each study area were analyzed for the best-fit stress tensor and the preferred nodal planes of failure for each focal mechanism. Inversion parameters of $s = 30^\circ$ and $d = 60^\circ$ were used for each study area because of moderate heterogeneity observed within the datasets, and default values of $\phi_1 = 60^\circ$ and $\phi_2 = 20^\circ$ were used for all inversions. My inversion also assumed Andersonian stress regimes when choosing trial tensors which restricted each of the individual principal stresses to near-vertical orientations during trial testing. Trials using non-Andersonian regimes resulted in a lower number of compatible results but with similar misfit values. Preferred nodal planes selected for each study area were subsequently extracted from the inversion results and plotted spatially. The strike and dip geometries and associated fault kinematics were observed for spatial relationships (such as alignment and/or clustering of fault planes with similar kinematics) as a means for identifying possible cross-structures. Results and interpretations from these analyses will be discussed in the following section.

V. Results and Interpretations

Seismicity Depth Distribution

Earthquake foci plotted for each study area reveal a large distribution of events at depth. Regions north and south of the upper-crustal promontory reveal a vast quantity of seismic events below the décollement, while seismicity in the promontory region is located mostly above the décollement at shallow levels (Figure 5). For the Sanyi, Pakua, and Chishan study areas, the depth to the décollement ranges from 5 - 8 km with the majority of the seismic activity occurring below this depth range. The lack of seismicity above the décollement level in these regions is suggestive of deformational processes within the full crust and does not support the development of cross-structures as suggested by the simplified model. Conversely, the Chiayi study area is characterized by a vast number of seismic events above the 8 km décollement level. Because active deformation is occurring in the shallow upper crust, the likelihood of developing cross-structures in this region is greater.

Focal Mechanism Deformation Styles

Uniform distributions of deformation styles within each of the study area ternary plots suggest kinematic heterogeneity within the datasets. Each of the study areas are represented by nearly equal amounts of normal, strike-slip and thrust focal mechanisms, along with a large number of oblique focal mechanisms, in accordance with the varying orientations of P, T, and B axes (Figure 6). However, in the Pakua study area, few strike-slip focal mechanisms are observed. Conversely, the Chishan study area is dominated by a mixed regime of thrust and strike-slip kinematics; normal faulting is almost entirely absent in this study area. Typical active collisional systems are expected to be dominated by compressional structures (i.e. thrust or

reverse faulting). However, these observed complexities in deformation styles suggest a more complicated deformation mechanism within the Taiwan fold-and-thrust belt.

Stress Inversion and Spatial Analysis Results

Results for the primary stress tensors derived from each stress inversion are presented in the following sections. In total, these primary tensors account for 76.3% of all focal mechanisms used in this study. Inversion results include the principal stress orientations, the preferred nodal planes of failure and inferred kinematic axes (Table 3). Inversion results for all of the focal mechanisms can be found in Appendix 1. Preferred nodal plane orientations are plotted in map-view and assessed for spatial and kinematic relationships.

Table 3. Summary of inversion input parameters and phase 1 inversion results.

	Input Parameters					Inversion Results (Phase 1)				
	# Input	$\phi 1$	$\phi 2$	s	d	# Output	$\sigma 1$	$\sigma 2$	$\sigma 3$	D
STFZ	161	60°	20°	30°	60°	115	281/13	127/76	013/06	0.1
PTFZ	314	60°	20°	30°	60°	203	300/75	187/06	096/13	0.2
CTFZ	289	60°	20°	30°	60°	242	295/12	089/76	204/06	0.4
ChiTFZ	189	60°	20°	30°	60°	167	267/13	177/02	078/77	0.3

Input - number of focal mechanisms put into the inversion. $\phi 1$ - angle of internal friction. $\phi 2$ - angle of residual friction (both control the normal-to-shear stress ratio). s - standard deviation of the angular misfit (s). d - threshold value of compatibility which is equal to the maximum angular misfit. # Output - number of focal mechanisms chosen from the optimal phase 1 inversion. $\sigma 1$ - trend/plunge of the maximum compressional axis. $\sigma 2$ - trend/plunge of the intermediate compressional axis. $\sigma 3$ - trend/plunge of the minimum compressional axis. D - Stress ratio defined as $D = (\sigma 2 - \sigma 3) / (\sigma 1 - \sigma 3)$.

Sanyi Study Area

For the Sanyi area, 161 earthquake focal mechanisms (322 nodal planes) were analyzed (Figure 7). The inversion yielded 115 compatible nodal planes representing 71% of the study area data. The inversion produced a stress ellipse with a vertical $\sigma 2$, west-trending maximum compression (281°), and north-trending minimum compression (013°). Kinematic axes show WNW-ESE directed compression and NNE-SSW directed extension suggestive of a strike-slip

regime. Rose diagrams of the preferred nodal plane dip directions reveal that the preferred nodal plane geometries are variable. Map-view distributions of strike-slip nodal planes also suggest variability in orientations, even at small scales.

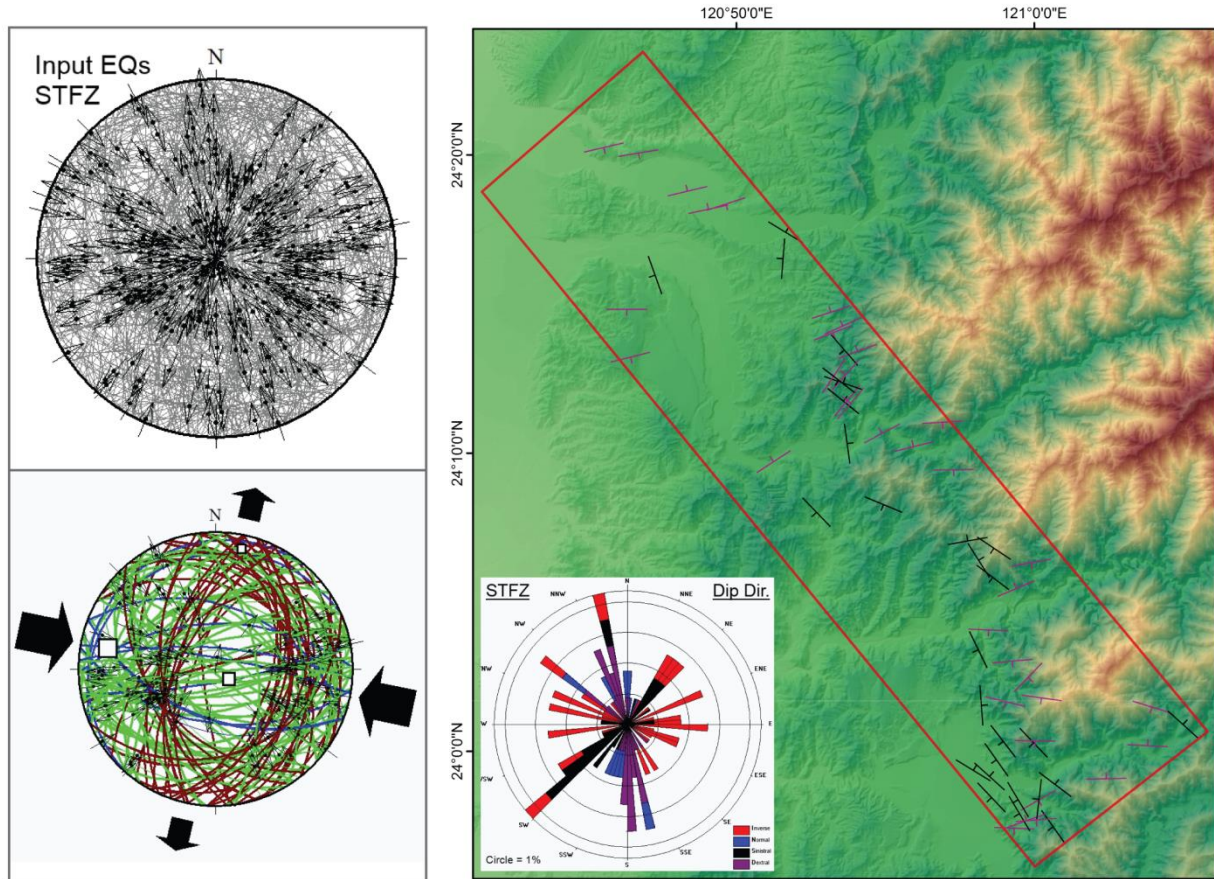


Figure 7. Sanyi study area stress inversion results. Stereonets: Equal-area, lower hemisphere stereonets. (Top) Input nodal planes from each focal mechanism. Thin black arrows - nodal plane slip vector. (Bottom) Best-fit stress tensor and preferred nodal planes derived from focal mechanism inversion. Large square - maximum compression axis. Medium square - intermediate compression axis. Small square - minimum compression axis. Red planes - thrust faults. Blue planes - normal faults. Green planes - strike-slip faults. Rose Diagram: Dip direction plots of the preferred nodal planes. Red - thrust fault. Blue - normal fault. Black - sinistral fault. Purple - dextral fault. Map: Spatial plot of oriented sinistral and dextral fault strike-dip symbols.

Analysis of the Sanyi study area reveals that the observed cross-structures in this zone do not represent a discrete zone of tear faulting but rather a zone of conjugate faulting. In terms of significant spatial relationships, neither the sinistral nor dextral nodal planes create a narrow,

through-going lineament/cluster in map-view. However, many of the sinistral nodal planes strike to the northwest and the dextral nodal planes strike toward the northeast. The configurations of these nodal planes, though dispersed across the zone, are consistent with conjugate fault geometries. As a conjugate system, these faults would accommodate northwest compression, similar to the convergence direction, and northward extension, suggestive of extrusion.

Pakua Study Area

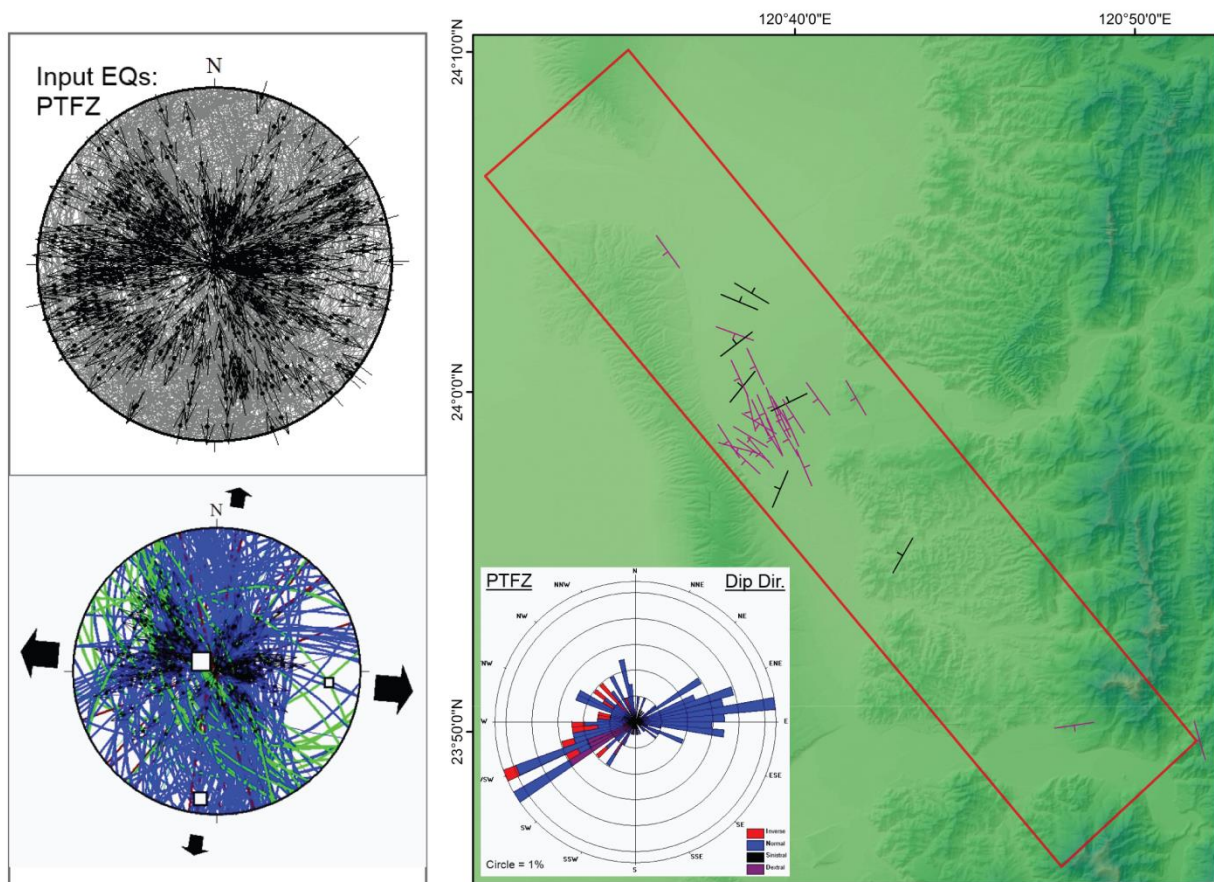


Figure 8. Pakua study area stress inversion results. Stereonets: Equal-area, lower hemisphere stereonets. (Top) Input nodal planes from each focal mechanism. Thin black arrows - nodal plane slip vector. (Bottom) Best-fit stress tensor and preferred nodal planes derived from focal mechanism inversion. Large square - maximum compression axis. Medium square - intermediate compression axis. Small square - minimum compression axis. Red planes - thrust faults. Blue planes - normal faults. Green planes - strike-slip faults. Rose Diagram: Dip direction plots of the preferred nodal planes. Red - thrust fault. Blue - normal fault. Black - sinistral fault. Purple - dextral fault. Map: Spatial plot of oriented sinistral and dextral fault strike-dip symbols.

For the Pakua area, 314 focal mechanisms (628 nodal planes) were analyzed (Figure 8). The inversion yielded 203 compatible nodal planes representing 64.6% of the study area data. The inversion produced a stress ellipse with a vertical σ_1 and east-trending minimum compression (096°). Kinematic axes show dominant east-west extension suggestive of a normal faulting regime. Rose diagrams of the preferred nodal plane dip directions reveal that the study area is largely characterized by NNW-trending normal faults dipping both east and west. Some dextral nodal planes are also observed parallel to the normal faults. Map-view distributions of preferred nodal planes along the northeastern flank of the Pakuashan Anticline show clusters of N-S trending normal faults.

Analysis of the Pakua area reveals that the region is dominated by normal faulting on the eastern flank of the Pakuashan anticline. The limited amount of strike-slip faulting in this region indicates that the study area is likely not a cross-structure as interpreted in previous studies. While the presence of normal faulting is an anomaly in this actively deforming part of the fold-and-thrust belt, I hypothesize that kinematics here may be related to the zone's proximity to the deformation front and Peikang High as material at the front is forced to ramp up over the high, potentially causing localized collapse behind the growing Pakuashan anticline.

Chiayi Study Area

For the Chiayi area, 289 earthquake focal mechanisms (578 nodal planes) were analyzed (Figure 9). The inversion yielded 242 compatible nodal planes representing 83.7% of the study area data. The inversion produced a stress ellipse with a vertical σ_2 , northwest-trending maximum compression (295°), and southwest-trending minimum compression (204°). Kinematic axes show NW-SE directed compression and NE-SW directed extension suggestive of a strike-slip regime. Rose diagrams of the preferred nodal plane dip directions reveal strong patterns of

consistently oriented preferred nodal planes. Sinistral nodal planes strike NNW, dextral nodal planes strike ENE, thrust nodal planes strike northeast, and normal nodal planes strike northwest. Map-view distributions of strike-slip nodal planes reveal a diffuse pattern of dextral nodal planes but a very narrow, linear zone of northwest trending preferred nodal planes.

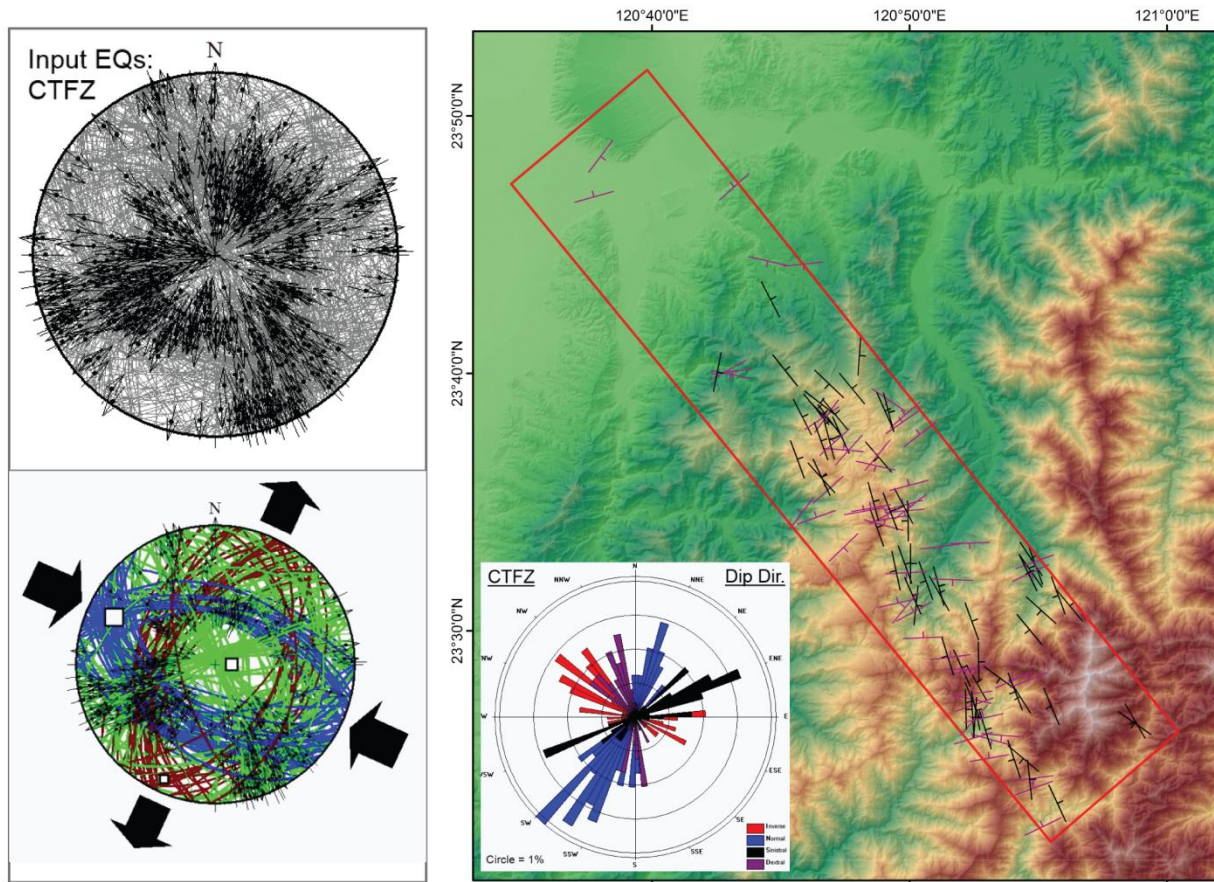


Figure 9. Chiayi study area stress inversion results. Stereonets: Equal-area, lower hemisphere stereonets. (Top) Input nodal planes from each focal mechanism. Thin black arrows - nodal plane slip vector. (Bottom) Best-fit stress tensor and preferred nodal planes derived from focal mechanism inversion. Large square - maximum compression axis. Medium square - intermediate compression axis. Small square - minimum compression axis. Red planes - thrust faults. Blue planes - normal faults. Green planes - strike-slip faults. Rose Diagram: Dip direction plots of the preferred nodal planes. Red - thrust fault. Blue - normal fault. Black - sinistral fault. Purple - dextral fault. Map: Spatial plot of oriented sinistral and dextral fault strike-dip symbols.

Analysis of the Chiayi study area suggests that the region is a cross-structure within the fold-and-thrust belt, consistent with previous studies. The inversion and spatial analyses indicate

that the zone is a N150E (330°) striking, sinistral fault zone, a difference of 10° (N140E) from that suggested by Deffontaines et al. [1997].

Chishan Study Area

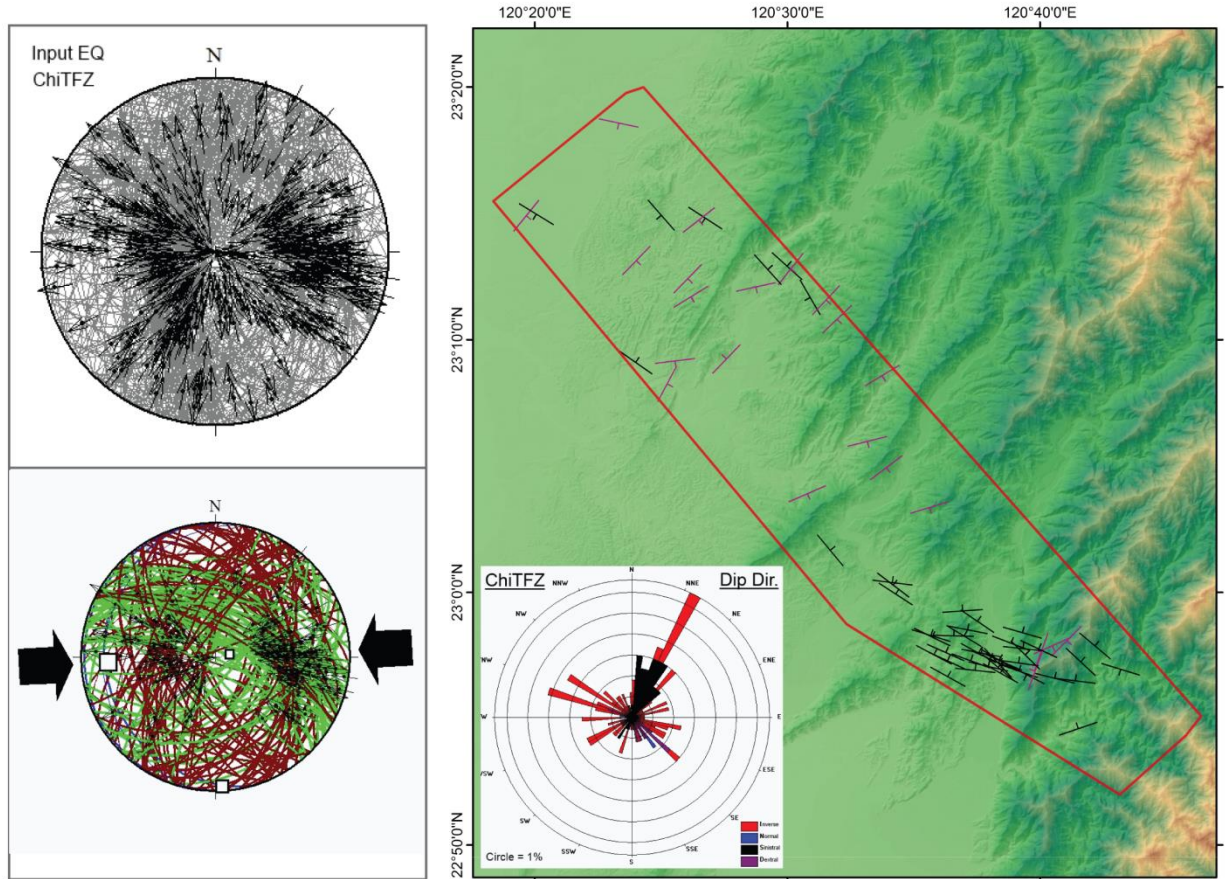


Figure 10. Chishan study area stress inversion results. Stereonets: Equal-area, lower hemisphere stereonets. (Top) Input nodal planes from each focal mechanism. Thin black arrows - nodal plane slip vector. (Bottom) Best-fit stress tensor and preferred nodal planes derived from focal mechanism inversion. Large square - maximum compression axis. Medium square - intermediate compression axis. Small square - minimum compression axis. Red planes - thrust faults. Blue planes - normal faults. Green planes - strike-slip faults. Rose Diagram: Dip direction plots of the preferred nodal planes. Red - thrust fault. Blue - normal fault. Black - sinistral fault. Purple - dextral fault. Map: Spatial plot of oriented sinistral and dextral fault strike-dip symbols.

For the Chishan study area, 189 earthquake focal mechanisms (378 nodal planes) were analyzed (Figure 10). The inversion yielded 167 compatible nodal planes representing 88.4% of the study area data. The inversion produced a stress ellipse with a vertical σ_3 and west-trending

maximum compression (267°). Kinematic axes show east-west compression suggestive of a thrust regime. Rose diagrams of the preferred nodal plane dip directions reveal that there is a dominant pattern of northwest-striking sinistral nodal planes and a dual pattern of northwest and northeast striking thrust nodal planes. Map-view distributions of strike-slip nodal planes show a tight cluster of northwest-striking, sinistral nodal planes at the southeastern end of the study area. Northeast-striking, dextral nodal planes are also observed, but with a disperse pattern.

Analysis of the Chishan study area suggest that the preferred nodal planes in this zone do not necessarily represent a cross-structure as suggested in previous studies. While it is true that there exists a tight cluster of sinistral focal mechanisms at the southeastern end of the study area, this cluster is limited to a small portion of the zone and shows little evidence of extending further. Additional evidence supporting this notion will be presented in the following section. Instead, the Chishan area better supports a zone of conjugate faulting. In addition to the many northwest-striking sinistral nodal planes in the study area, some northeast-striking dextral nodal planes are also observed. The configurations of these nodal planes, though diffuse across the zone, are fairly consistent with conjugate fault geometries. As a conjugate system, these faults would accommodate east-west compression and north-south extension, suggestive of extrusion toward the southern Tainan Basin.

VI. Margin Control on the Development of the Fold-and-Thrust Belt

The along-strike structural configuration of the Chinese continental margin has posed a major control on the geometry and kinematics of the Taiwan fold-and-thrust belt. While a lower crustal promontory has been evidenced in topographic data to cause the development of a major recess in the orogen, it is the margin geometry at upper crustal levels that is dictating most of the

contemporary growth of the fold-and-thrust belt. The geometry of the Peikang High and bounding Tashi and Tainan Basins has caused the fold-and-thrust belt to develop a curvilinear pattern of salients and recesses in the shallow foreland as it propagates westward and mimics the shape of the margin. This irregularly shaped orogen provides a favorable environment for the development of cross-structures in the collisional hangingwall [Marshak, 2004]. However, while previous studies have suggested the existence of four prominent cross-structures in the Taiwan fold-and-thrust belt, my analysis of earthquake seismicity and focal mechanisms suggests that the only evident, through-going tear fault of these four is the Chiayi cross-structure. This is supported by both the shallow distribution of earthquake events and the linear zone of sinistral nodal planes determined during analysis.

The Chiayi cross-structure serves as a necessary kinematic link that connects the northern and southern portions of the fold-and-thrust belt as they deform around the crustal promontory. Inversion results from the Sanyi and Chishan cross-structures indicate that across the Chiayi tear fault, the fold-and-thrust belt is deforming under two somewhat different stress regimes: to the north, deformation occurs under a northwest compressional regime, approximately normal to the point of maximum curvature of the northern salient; to the south, a westward compressional regime is causing deformation along oblique thrust faults. In both locations however, preferred nodal plane orientations suggest that deformation is being accommodated on a network of conjugate faults. These conjugate fault systems could be facilitating extrusion north and south of the promontory. Extrusion of orogenic material has been suggested for several locations across the Western Foothills [Angelier, 2009; Fuh *et al.*, 1997; Gourley, 2006; J-C Hu *et al.*, 2007] and has been proposed to occur due to the pinning of orogenic material against the margin during collision [Angelier, 2009; Teng, 1996]. Furthermore, the original cross-structure study by

Deffontaines et al. [1997] actually indicates this conjugate configuration; the drainage anomalies indicate a second pattern of cross-structures oriented approximately east-west (Figure 11). Several of these east-west structures have been mapped across the fold-and-thrust belt [Brown et al., 2012; Lacombe et al., 1999; Lee et al., 2002; Liu et al., 1997].

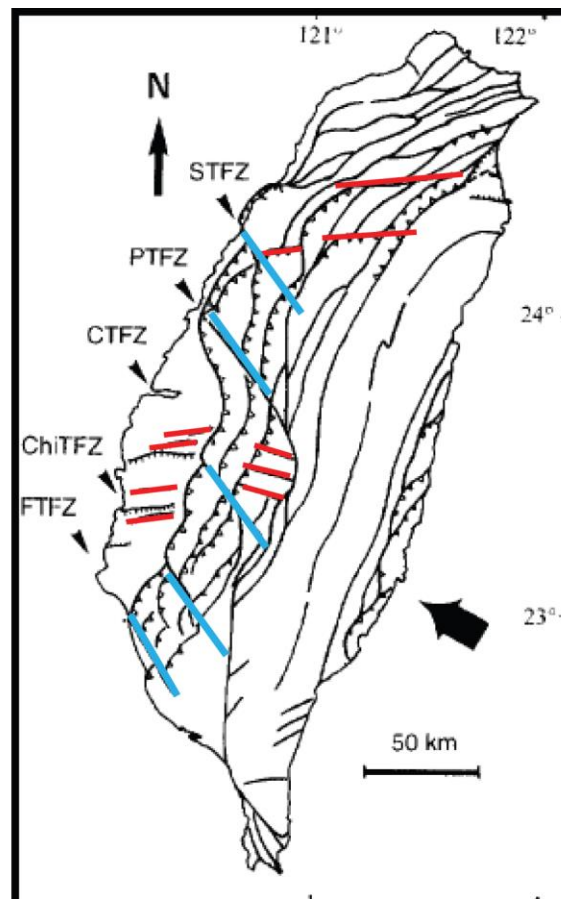


Figure 11. Drainage anomaly map of conjugate faults (from Deffontaines et al., 1997. Blue lines - N140E trending cross-structures evaluated in this study. Red lines - east-west trending cross-structures also delineated in the drainage anomalies. The observed geometry of these two sets of cross-structures are ideally oriented to produce conjugate fault sets.

Additionally, the Chiayi cross-structure is ideally located within the fold-and-thrust belt and in agreement with the simplified model. This structure parallels the northern edge of the Peikang High and foreland sediments marking a transition in basin fill from thick sediments in the Tashi Basin to thinned sediments above the Peikang High. Analog models suggest that these

types of cross-structures can develop in this configuration given lateral changes in sediment thickness [Lacombe *et al.*, 1999; Mouthereau *et al.*, 1999]. Because these lateral changes in sediment thicknesses exist in the Chiayi area, there is a high probability that such an accommodation structure would develop, which we now evidence in the focal mechanism inversion results. The Chiayi cross-structure also connects the northern and southern segments of the fold-and-thrust belt, facilitating its growth into the observed sigmoidal shape. It has been suggested that the necessity for this sigmoidal shape comes from the differential rates of advancement from north to south [Ching *et al.*, 2011; J C Hu *et al.*, 2001; Yu *et al.*, 1997].

While the Chiayi cross-structure is the only tear fault of note in the inversion results, further consideration should be given to a second potential structure in this region. This candidate structure is located to the northeast of the Chiayi cross-structure along the southern extent of the Shuilikeng Fault, the western bounding fault of the Hsüehshan Range (Figure 12). The Shuilikeng Fault defines a lithologic boundary between the slates of the Hsüehshan Range and the sandstones of the western foothills suggesting a fair amount of displacement along the zone. The parallel orientation of this candidate structure to the Chiayi cross-structure and the similar location at the southern end of an arcuate fault trace, coupled with the obviously large amount of time and displacement along the Shuilikeng Faults, leads me to hypothesize that candidate structure was developed at an older period of orogenic growth. If the southern extension of the Shuilikeng Fault is in fact a paleo-tear fault zone, then this would suggest that advancement of the fold-and-thrust belt over the crustal promontory is accommodated by a southward propagating set of en echelon tear faults that develop as the collision continues to ramp over the Peikang High. However, more work is needed to better understand the nature of this candidate fault zone.

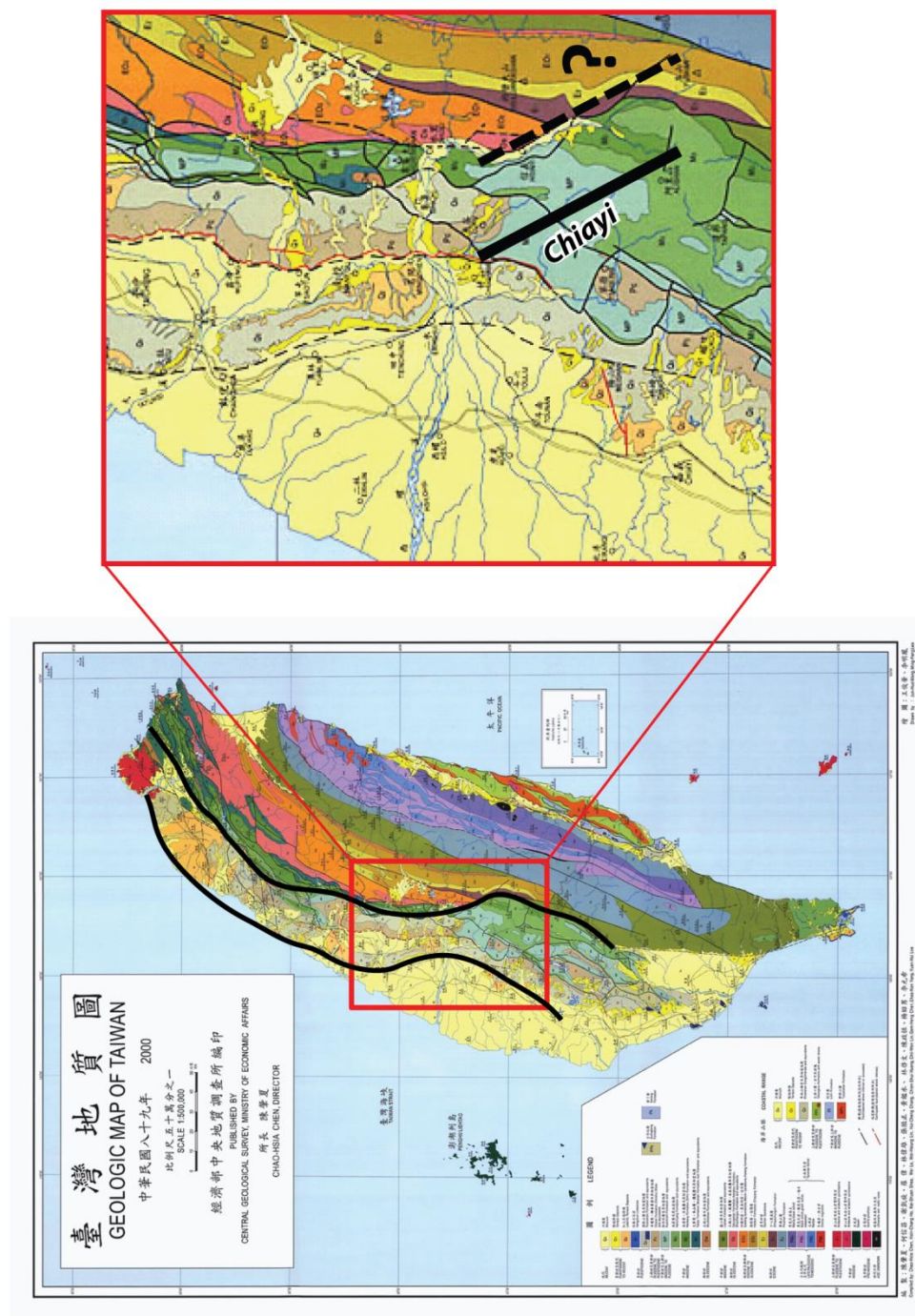


Figure 12. Geologic map of Taiwan with suggested tear faults. (Left) Island-wide map of geology. Black lines - general trace of northern salient following the Chenghua frontal thrust and the Shuilikeng Fault. Red box - focus area for the second diagram. (Right) Zoom of geologic map in central Taiwan at the southern end of the salient. Solid black line - interpreted location of the Chiayi tear fault. Dashed black line - hypothesized paleo-tear fault from the development of the Hsuehshan Range. Location was chosen from the abrupt break in geology in a trend similar to the Chiayi fault.

In sum, development of the Taiwan fold-and-thrust belt can be described by three deformation patterns related to the geometry of the Chinese continental margin (Figure 13). The cross-structures north of the promontory represent a zone of conjugate faulting that facilitates the extrusion of material to the northeast into the Tashi Basin. The central portion of Taiwan represents a transition region involved in collision with the complex continental margin promontory. This domain accommodates the differential propagation of the northern and southern fold-and-thrust belt using a propagating series of NW-trending, en echelon tear faults.

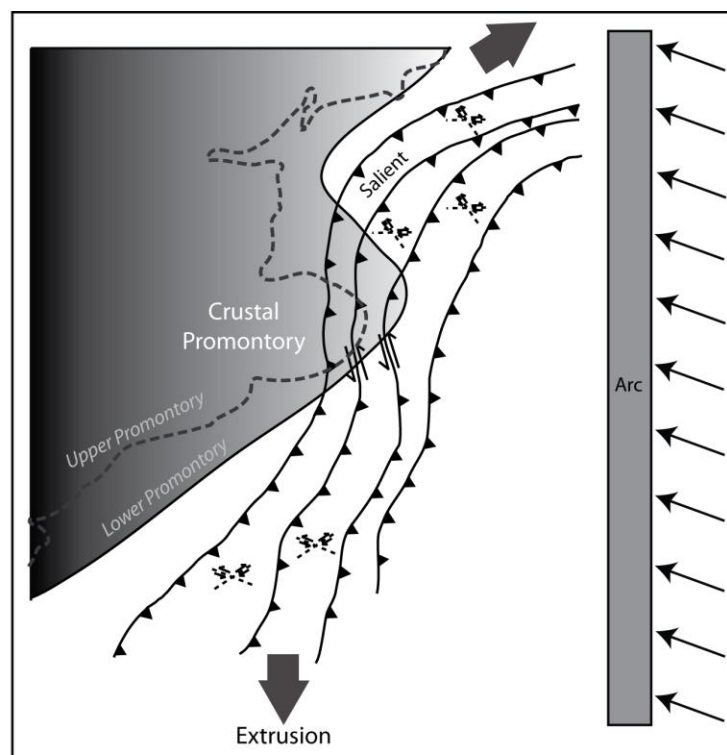


Figure 13. Oblique arc-continent collision model for fold-and-thrust belt deformation around a crustal promontory in Taiwan. Grey gradient polygon - lower crustal promontory. Dashed line - upper-crustal promontory. Black barbed lines - traces of thrust sheets with barbs on the hangingwall. Dashed crossed lines - conjugate fault regions with sense of slip indicated by half arrows. Thick grey arrows - extrusion direction indicators. Thin filled arrows - convergence direction of the arc.

Similar to the northern domain, conjugate faulting is also observed in the southern domain. Here, conjugate fault systems develop with faults parallel and oblique to the margin and thrust sheets

and facilitate extrusion of material southward into the Tainan Basin. Of all the cross-structures identified across the fold-and-thrust belt, only the Chiayi study area is a tear fault zone.

VII. Conclusion

The fundamental process of orogenic development is often over-simplified by traditional models by failing to take into consideration along-strike irregularities of the collisional footwall. Irregular footwall geometries are fairly common and can cause the development of curvilinear fold-and-thrust belts during collision. In Taiwan, the geometry of the Chinese continental margin has been suggested to facilitate the development of several cross-structures, transverse structures that trend oblique to the structural grain of the orogen, within the fold-and-thrust belt. In total, at least six cross-structures have been suggested by previous studies. These cross-structures have been discussed in several geomorphic, geologic, and geophysical investigations focusing on surface and shallow crustal characteristics. For this study, a catalog of earthquake seismicity and earthquake focal mechanisms were used to evaluate and characterize the cross-structures at depth. Using the Gauss inversion method, best-fit stress tensors were derived for each study area and the associated preferred nodal planes of failure were extracted for spatial analyses. Results suggest that deformation patterns north and south of the crustal promontory are characterized by systems of conjugate faulting that facilitate brittle extrusion of foreland material as the orogen becomes caught up in collision with the irregular margin. The region around the promontory represents a narrow zone of southward propagating, en echelon tear faults that accommodate differential displacement of the advancing thrust sheets through time. Tear faulting is limited to the upper crustal layers and are necessary for the orogen to advance over the promontory.

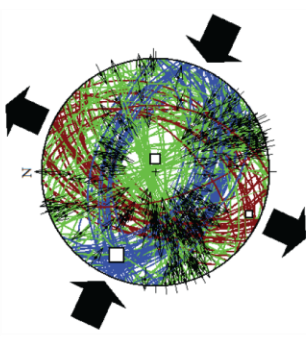
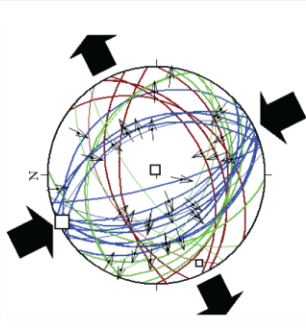
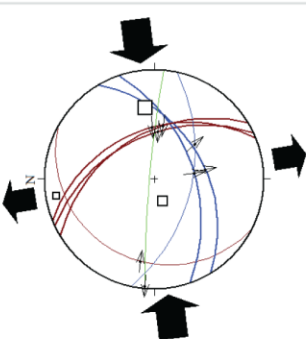
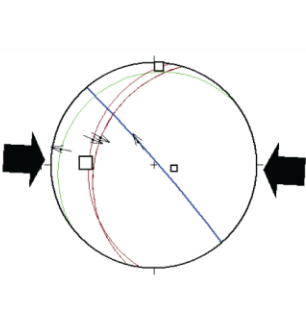
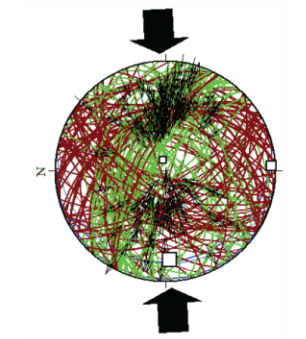
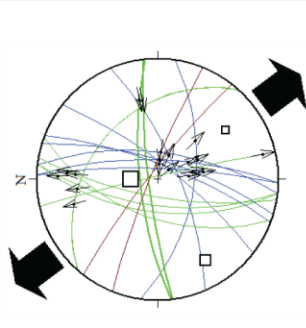
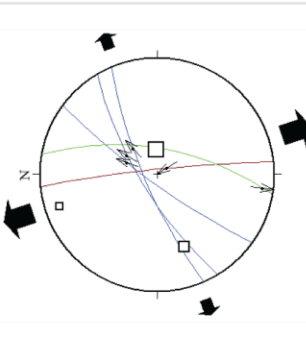

VIII. Appendix

Summary of inversion results for all phases.

STFZ Inversion									
#	115	32	12	2	1				
σ_1	226/76	077/75	164/23	226/76	015/02				
σ_2	339/06	179/03	064/22	339/06	105/02				
σ_3	071/13	269/14	295/57	071/13	240/87				
D	0.6	0.1	0.2	0.6	1				
PTFZ Inversion									
#	203	85	19	7	1				
σ_1	300/75	076/02	170/12	083/23	262/65				
σ_2	187/06	346/02	262/12	183/22	062/24				
σ_3	096/13	211/87	034/73	312/57	155/08				
D	0.2	0.4	0.1	0.2	0.1				

Stereonets: Equal-area, lower hemisphere stereonet. Red great circle - thrust fault. Blue great circle - normal fault. Green great circle - strike-slip fault (both types). Large square - maximum compression axis. Medium square - intermediate compression axis. Small square - minimum compression axis. Table: # - number of nodal planes in each phase. σ_1 - maximum compression axis trend and plunge. σ_2 - intermediate compression axis trend and plunge. σ_3 - minimum compression axis trend and plunge. D - stress ratio defined as $D = (\sigma_2 - \sigma_3) / (\sigma_1 - \sigma_3)$.

Summary of inversion results for all phases.

CTFZ Inversion									
#	242	33	9	4					
σ_1	295/12	334/02	083/23	002/23					
σ_2	089/76	082/84	248/66	093/02					
σ_3	204/06	244/06	351/06	188/67					
D	0.4	0.4	0.3	0.6					
ChITFZ Inversion									
#	167	18	5						
σ_1	267/13	003/65	089/65						
σ_2	177/02	239/14	249/24						
σ_3	078/77	144/20	342/08						
D	0.3	0.5	0.2						

Stereonets: Equal-area, lower hemisphere stereonet. Red great circle - thrust fault. Blue great circle - normal fault. Green great circle - strike-slip fault (both types). Large square - maximum compression axis. Medium square - intermediate compression axis. Small square - minimum compression axis. Table: # - number of nodal planes in each phase. σ_1 - maximum compression axis trend and plunge. σ_2 - intermediate compression axis trend and plunge. σ_3 - minimum compression axis trend and plunge. D - stress ratio defined as $D = (\sigma_2 - \sigma_3) / (\sigma_1 - \sigma_3)$.

IX. References

- Angelier, J. (1990), Inversion of field data in fault tectonics to obtain the regional stress—III. A new rapid direct inversion method by analytical means, *Geophysical Journal International*, 103(2), 363-376.
- Angelier, J. (2009), Does extrusion occur at both tips of the Taiwan collision belt? Insights from active deformation studies in the Ilan Plain and Pingtung Plain regions, *Tectonophysics*, 466, 356-376.
- Angelier, J., A. Tarantola, B. Valette, and S. Manoussis (1982), Inversion of field data in fault tectonics to obtain the regional stress—I. Single phase fault populations: a new method of computing the stress tensor, *Geophysical Journal of the Royal Astronomical Society*, 69(3), 607-621.
- Brown, D., J. Alvarez-Marron, M. Schimmel, Y. M. Wu, and G. Camanni (2012), The structure and kinematics of the central Taiwan mountain belt derived from geological and seismicity data, *Tectonics*, 31(5).
- Brown, D., P. D. Ryan, J. Afonso, D. Boutelier, J. Burg, T. Byrne, A. Calvert, F. Cook, S. DeBari, and J. Dewey (2011), *Arc-continent collision: The making of an orogen*, Springer.
- Byrne, T., Y.-C. Chan, R.-J. Rau, C.-Y. Lu, Y.-H. Lee, and Y.-J. Wang (2011), The arc-continent collision in Taiwan, in *Arc-Continent Collision*, edited, pp. 213-245, Springer.
- Carey-Gailhardis, E., and J. Louis Mercier (1987), A numerical method for determining the state of stress using focal mechanisms of earthquake populations: application to Tibetan teleseisms and microseismicity of Southern Peru, *Earth and Planetary Science Letters*, 82(1), 165-179.
- Célérier, B., A. Etchecopar, F. Bergerat, P. Vergely, F. Arthaud, and P. Laurent (2012), Inferring stress from faulting: from early concepts to inverse methods, *Tectonophysics*, 581, 206-219.
- Cheng, W.-B. (2004), Crustal structure of the high magnetic anomaly belt, Western Taiwan, and its implications for continental margin deformation, *Marine Geophysical Researches*, 25(1-2), 79-93.
- Ching, K.-E., R.-J. Rau, K. M. Johnson, J.-C. Lee, and J.-C. Hu (2011), Present-day kinematics of active mountain building in Taiwan from GPS observations during 1995–2005, *Journal of Geophysical Research*, 116(B9), B09405.
- Clift, P. D., H. Schouten, and A. E. Draut (2003), A general model of arc-continent collision and subduction polarity reversal from Taiwan and the Irish Caledonides, *Geological Society, London, Special Publications*, 219(1), 81-98.
- Davis, D., J. Suppe, and F. A. Dahlen (1983), Mechanics of Fold-and-Thrust Belts and Accretionary Wedges *Journal of Geophysical Research*, 88(B2), 1153-1172.
- Deffontaines, B., J. C. Lee, J. Angelier, J. Carvalho, and J. P. Rudant (1994), New geomorphic data on the active Taiwan orogen: A multisource approach, *Journal of Geophysical Research: Solid Earth (1978–2012)*, 99(B10), 20243-20266.
- Deffontaines, B., O. Lacombe, J. Angelier, H. Chu, F. Mouthereau, C. Lee, J. Deramond, J. Lee, M. Yu, and P. Liew (1997), Quaternary transfer faulting in the Taiwan Foothills: evidence from a multisource approach, *Tectonophysics*, 274(1), 61-82.
- Ding, Z.-Y., Y.-Q. Yang, Z.-X. Yao, and G.-H. Zhang (2001), A thin-skinned collisional model for the Taiwan orogeny, *Tectonophysics*, 332(3), 321-331.
- Frohlich, C. (1992), Triangle diagrams: ternary graphs to display similarity and diversity of earthquake focal mechanisms, *Physics of the Earth and Planetary Interiors*, 75(1), 193-198.

Fuh, S.-C., C.-S. Liu, N. Lundberg, and D. L. Reed (1997), Strike-slip faults offshore southern Taiwan; implications for the oblique arc-continent collision processes, *Tectonophysics*, 274, 25-39.

Gephart, J. W. (1985), Principal stress directions and the ambiguity in fault plane identification from focal mechanisms, *Bulletin of the Seismological Society of America*, 75(2), 621-625.

Gephart, J. W., and D. W. Forsyth (1984), An improved method for determining the regional stress tensor using earthquake focal mechanism data: application to the San Fernando earthquake sequence, *Journal of Geophysical Research: Solid Earth (1978–2012)*, 89(B11), 9305-9320.

Gourley, J. R. (2006), Syn-tectonic extension and lateral extrusion in Taiwan: the tectonic response to a basement high promontory, University of Connecticut, Storrs.

Harmsen, S., and A. Rogers (1986), Inferences about the local stress field from focal mechanisms: Applications to earthquakes in the southern Great Basin of Nevada, *Bulletin of the Seismological Society of America*, 76(6), 1560-1572.

Ho, C. S. (1976), Foothills tectonics of Taiwan, *Bull. Geol. Surv. Taiwan*, 25, 9-28.

Ho, C. S. (1986), A synthesis of the geologic evolution of Taiwan, *Tectonophysics*, 125, 1-16.

Hsu, S.-K., C.-S. Liu, C.-T. Shyu, S.-Y. Liu, J.-C. Sibuet, S. Lallemant, C. Wang, and D. Reed (1998), New gravity and magnetic anomaly maps in the Taiwan-Luzon region and their preliminary interpretation, *TAO*, 9(3), 509-532.

Hu, J.-C., C.-S. Hou, L.-C. Shen, Y.-C. Chan, R.-F. Chen, C. Huang, R.-J. Rau, K. H.-H. Chen, C.-W. Lin, and M.-H. Huang (2007), Fault activity and lateral extrusion inferred from velocity field revealed by GPS measurements in the Pingtung area of southwestern Taiwan, *Journal of Asian Earth Sciences*, 31(3), 287-302.

Hu, J. C., S. B. Yu, J. Angelier, and H. T. Chu (2001), Active deformation of Taiwan from GPS measurements and numerical simulations, *Journal of Geophysical Research: Solid Earth (1978–2012)*, 106(B2), 2265-2280.

Huang, Q., and J. Angelier (1989), Inversion of field data in fault tectonics to obtain the regional stress—II. Using conjugate fault sets within heterogeneous families for computing palaeostress axes, *Geophysical Journal International*, 96(1), 139-149.

Huang, S.-T., K.-M. Yang, J.-C. Wu, H.-H. Ting, C.-J. Lee, W.-W. Mei, and H.-H. Hsu (2004), On-land fault zone structure and crustal deformation survey of Taiwan (5/5) – Analysis of the subsurface structures in the Western Foothill: Fault activity observation and earthquake potential evaluation. *Rep.*, 72 pp, Taiwan Central Geological Survey.

Kao, H., and W.-P. Chen (2000), The Chi-Chi earthquake sequence: Active, out-of-sequence thrust faulting in Taiwan, *Science*, 288(5475), 2346-2349.

Lacombe, O., F. Mouthereau, J. Angelier, and B. Deffontaines (2001), Structural, geodetic and seismological evidence for tectonic escape in SW Taiwan, *Tectonophysics*, 333(1), 323-345.

Lacombe, O., F. Mouthereau, B. Deffontaines, J. Angelier, H. Chu, and C. Lee (1999), Geometry and Quaternary kinematics of fold-and-thrust units of southwestern Taiwan, *Tectonics*, 18(6), 1198-1223.

Lee, J.-C., and Y.-C. Chan (2007), Structure of the 1999 Chi-Chi earthquake rupture and interaction of thrust faults in the active fold belt of western Taiwan, *Journal of Asian Earth Sciences*, 31(3), 226-239.

Lee, J.-C., C.-Y. Lu, H.-T. Chu, B. Delcaillau, J. Angelier, and B. Deffontaines (1996), Active deformation and paleostress analysis in the Pakua Anticline area of western Taiwan, *Terrestrial, Atmospheric and Oceanic Sciences*, 7(4), 431-446.

- Lee, J.-C., H.-T. Chu, J. Angelier, Y.-C. Chan, J.-C. Hu, C.-Y. Lu, and R.-J. Rau (2002), Geometry and structure of northern surface ruptures of the 1999 Mw= 7.6 Chi-Chi Taiwan earthquake: influence from inherited fold belt structures, *Journal of Structural Geology*, 24(1), 173-192.
- Lin, A., A. Watts, and S. Hesselbo (2003), Cenozoic stratigraphy and subsidence history of the South China Sea margin in the Taiwan region, *Basin Research*, 15(4), 453-478.
- Liu, C.-S., I. L. Huang, and L. S. Teng (1997), Structural features off southwestern Taiwan, *Marine Geology*, 137(3), 305-319.
- Macedo, J., and S. Marshak (1999), Controls on the geometry of fold-thrust belt salients, *Geological Society of America Bulletin*, 111(12), 1808-1822.
- Marshak, S. (2004), Salients, Recesses, Arcs, Oroclines, and Syntaxes A Review of Ideas Concerning the Formation of Map-view Curves in Fold-thrust Belts.
- Michael, A. J. (1987), Use of focal mechanisms to determine stress: a control study, *Journal of Geophysical Research: Solid Earth (1978–2012)*, 92(B1), 357-368.
- Mirakian, D. C., J. M. Crespi, T. B. Byrne, C. Huang, W. B. Ouimet, and J. C. Lewis (2012), Tectonic implications of nonparallel topographic and structural curvature in the higher elevations of an active collision zone, Taiwan, *Lithosphere*, 5(1), 49-66.
- Mouthereau, F., and O. Lacombe (2006), Inversion of the Paleogene Chinese continental margin and thick-skinned deformation in the Western Foreland of Taiwan, *Journal of Structural Geology*, 28(11), 1977-1993.
- Mouthereau, F., O. Lacombe, B. Deffontaines, J. Angelier, and S. Brusset (2001), Deformation history of the southwestern Taiwan foreland thrust belt: insights from tectono-sedimentary analyses and balanced cross-sections, *Tectonophysics*, 333(1), 293-318.
- Mouthereau, F., O. Lacombe, B. Deffontaines, J. Angelier, H. Chu, and C. Lee (1999), Quaternary transfer faulting and belt front deformation at Pakuashan (western Taiwan), *Tectonics*, 18(2), 215-230.
- Rau, R.-J., and F. T. Wu (1995), Tomographic imaging of lithospheric structures under Taiwan, *Earth and Planetary Science Letters*, 133(3), 517-532.
- Rau, R.-J., K.-E. Ching, J.-C. Hu, and J.-C. Lee (2008), Crustal deformation and block kinematics in transition from collision to subduction: Global positioning system measurements in northern Taiwan, 1995-2005, *Journal of Geophysical Research*, 113(B09404, doi:10.1029/2007JB005414).
- Suppe, J. (1981), Mechanics of mountain building and metamorphism in Taiwan, *Mem. Geol. Soc. China*, 4, 67-89.
- Taylor, B., and D. E. Hayes (1983), Origin and history of the South China Sea basin, *The Tectonic and Geologic Evolution of Southeast Asian Seas and Islands: Part 2*, 23-56.
- Teng, L. S. (1996), Extensional collapse of the Northern Taiwan mountain belt, *Geology*, 24(10), 949-952.
- Wang, C., C.-P. Huang, L.-Y. Ke, W.-J. Chien, S.-K. Hsu, C.-T. Shyu, W.-B. Cheng, C.-S. Lee, and L. S. Teng (2002), Formation of the Taiwan Island as a solitary wave along the Eurasian continental plate margin: magnetic and seismological evidence, *TAO*, 13(3), 339-354.
- Yu, S.-B., H.-Y. Chen, and L.-C. Kuo (1997), Velocity field of GPS stations in the Taiwan area, *Tectonophysics*, 274(1), 41-59.

Žalohar, J., and M. Vrabec (2007), Paleostress analysis of heterogeneous fault-slip data: the Gauss method, *Journal of Structural Geology*, 29(11), 1798-1810.

Zoback, M. L. (1992), Stress field constraints on intraplate seismicity in eastern North America, *Journal of Geophysical Research: Solid Earth (1978–2012)*, 97(B8), 11761-11782.